Hydrogeology and Mechanics of Subduction Zone Forearcs: Fluid Flow and Pore Pressure

Demian M. Saffer[1] and Harold J. Tobin[2]

[1]Department of Geosciences, The Pennsylvania State University, University Park, Pennsylvania 16802; email: demian@psu.edu

[2]Department of Geoscience, University of Wisconsin-Madison, Madison, Wisconsin 53706; email: htobin@geology.wisc.edu

Annu. Rev. Earth Planet. Sci. 2011. 39:157–86

First published online as a Review in Advance on February 2, 2011

The *Annual Review of Earth and Planetary Sciences* is online at earth.annualreviews.org

This article's doi:
10.1146/annurev-earth-040610-133408

0084-6597/11/0530-0157$20.00

Keywords

fault strength, overpressure, accretionary wedge, seismogenic zone, permeability

Abstract

At subduction zones, fluid flow, pore pressure, and tectonic processes are tightly interconnected. Excess pore pressure is driven by tectonic loading and fluids released by mineral dehydration, and it has profound effects on fault and earthquake mechanics through its control on effective stress. The egress of these overpressured fluids, which is in part governed by the presence of permeable fault zones, is a primary mechanism of volatile and solute transport to the oceans. Recent field measurements, new constraints gained from laboratory studies, and numerical modeling efforts have led to a greatly improved understanding of these coupled processes. Here, we summarize the current state of knowledge of fluid flow and pore pressure in subduction forearcs, and focus on recent advances that have quantified permeability architecture, fluxes, the nature and timing of transience, and pressure distribution, thus providing new insights into the connections between fluid, metamorphic, mechanical, and fault slip processes.

1. INTRODUCTION

Permeability (k): intrinsic property of a geologic medium describing its ability to transmit fluid, measured in units of L^2; related to the size and degree of interconnection of pore space

VLFE: very low-frequency earthquakes

ETS: episodic tremor and slip

SSE: slow slip events

Fluids and tectonic processes are inextricably interwoven. Tectonic processes drive fluid pressures and pore fluid geochemical evolution through loading and heating, and they modulate fluid escape by modifying permeability through faulting and deformation. Conversely, pore pressure and lithological alteration associated with fluid transport govern deformation and faulting. In subduction zones, fluids are released through compaction and mineral dehydration as sediments are buried and heated, and pore pressures rise and fluids are expelled as a result. Fluid flow associated with subsurface pore pressures is one primary agent of volatile and solute mass fluxes out of forearcs (e.g., Hacker 2008, Hensen et al. 2004, Kastner et al. 1991, Sahling et al. 2008). Fluid pressure affects a wide range of faulting processes through its control on effective normal stress, including absolute fault strength (e.g., Davis et al. 1983, Hubbert & Rubey 1959, Magee & Zoback 1993, Rice 1992, Tobin & Saffer 2009) and the propagation of rupture and migration of microseismicity (e.g., Johnson & McEvilly 1995, Tsuru et al. 2005). Elevated pore pressure has also been invoked as a key factor governing a host of recently discovered fault slip behaviors along subduction thrusts, including very low-frequency earthquakes (VLFE), episodic tremor and slip (ETS), and slow slip events (SSE) (e.g., Audet et al. 2009, Ito & Obara 2006, Kodaira et al. 2004, Liu & Rice 2007, Obana & Kodaira 2009).

In the past 10–15 years, data from advanced 2D and 3D seismic imaging and drilling, instrumentation at the seabed and within boreholes, new geodetic and seismological observations, and coordinated sustained efforts at individual margins have revealed new connections between fluid, metamorphic, and mechanical processes. One major advance has come from improved constraints on the permeability architecture of forearcs through laboratory measurements conducted on core samples (Gamage & Screaton 2006, Saffer & McKiernan 2005, Zwart et al. 1997), well tests enabled by scientific ocean drilling (Bekins et al. 2011, Fisher & Zwart 1996, Screaton et al. 2000, Screaton et al. 1995), and estimates derived from detailed numerical modeling studies (e.g., Bekins et al. 1995, Spinelli et al. 2006). In conjunction with field campaigns that have extensively documented seafloor vent-site distributions and flow rates (e.g., Hensen et al. 2004, Ranero et al. 2008, Sahling et al. 2008), this clearer picture of forearc permeability architecture has led to improved constraints on fluid flow rates and hydrologic budgets. A second major advance has accompanied the emergence of long-term monitoring tools for seafloor and borehole deployment; these tools have brought the ability to continuously record in situ pore pressure and fluid chemistry, revealing new links between fluid flow, pore pressure, surface seeps, and fault slip (e.g., Brown et al. 2005, Davis et al. 2006, Solomon et al. 2009). A third major step forward has come from advances in geophysical imaging and resolution of the seismic velocity structure of the crust and upper mantle, coupled with drilling. These advances have allowed rigorous quantification of anomalous fluid volume and pore fluid pressure (e.g., Calahorrano et al. 2008, Saffer 2003, Screaton et al. 2002, Tobin & Saffer 2009) as well as qualitative detection of possible pore fluid anomalies governing newly documented modes of fault slip such as SSE, VLFE, and ETS (Audet et al. 2009, Kodaira et al. 2004, Ito & Obara 2006, Kato et al. 2010, Song et al. 2009). These studies have provided a basis for understanding and quantifying the factors that control excess pore pressure magnitude and distribution and, ultimately, absolute fault strength (see sidebar, Excess Pore Pressure).

These recent strides have provided a clearer and increasingly complete understanding of fluid flow and pore pressure in subduction zones and their roles in volatile budgets and fault mechanical behavior. In this review, we discuss these fundamental new findings and summarize the present state of knowledge of fluids and tectonic processes in subduction zone forearcs, drawing on examples from several extensively studied margins (**Figure 1**). We focus on the outer subduction zone, from the deformation front to the brittle-ductile transition zone where the plate interface is

EXCESS PORE PRESSURE

Excess pore pressure, also known as overpressure, is pore fluid pressure above the hydrostatic pressure, indicative of disequilibrium driven by geologic mechanisms such as mechanical loading or metamorphic dehydration that outpace fluid escape and thus lead to trapping of fluids.

conditionally stable for frictional slip and commonly exhibits tremor, slow slip, and low-frequency earthquakes (LFE) (**Figure 2**). For simplicity, we refer to this region as the forearc. First, in Section 2, we review and summarize the fundamental hydrogeological processes that govern the movement and trapping of fluids. Second, in Section 3, we explore the state of understanding of fluid flow, including rates, volumes, spatial distribution and heterogeneity, and exchange with the overlying ocean and deeper regions of the crust and mantle. Section 4 examines the generation and effects of excess pore fluid pressure, with an emphasis on fault strength and slip behaviors, including proposed links between pore fluid pressure and VLFE, SSE, and ETS. Through this review, we address the linked questions: Where do fluids come from, where do they go, how are they held in place, and what effects do they have on rock mechanical processes?

2. FLUIDS IN SUBDUCTION FOREARCS: BACKGROUND AND KEY CONCEPTS

The general equation describing subsurface fluid flow is given by combining Darcy's Law and the conservation of fluid mass:

$$\rho S_s \frac{\partial p}{\partial t} - \nabla \left[\left(\frac{k\rho}{\nu} \right) \cdot (\nabla p - \rho g) \right] - \rho \Gamma = 0 \qquad (1)$$

where ρ is fluid density, S_s is specific storage in units of inverse pressure, p is fluid pressure, t is time, k is permeability, ν is fluid viscosity, and Γ represents geologic processes acting as distributed sources or sinks of fluid pressure (expressed in units of $V_{H2O}/V_{ROCK}\ s^{-1}$). These geologic processes, termed geologic forcing, include actual sources of fluid volume (e.g., fluid release by mineral dehydration reactions) and those that act as virtual fluid sources (e.g., disequilibrium compaction) (Bethke 1986; also see Neuzil 1995 and references therein).

On the basis of Equation 1, Neuzil (1995) developed a simple criterion describing the generation and maintenance of anomalous pore fluid pressures as a balance between the magnitude of geologic forcing (Γ) and the rate of pore pressure diffusion, which is in turn controlled by the hydraulic conductivity (K) and drainage path length (L), to show that excess pore fluid pressures (defined by a hydraulic head gradient of unity) are likely if the dimensionless quantity $\Gamma L/K > 1$. This conceptual model is applicable in a wide range of geologic settings, including sedimentary basins, upper crust undergoing prograde metamorphism, and accretionary wedges and underthrusting sediment (e.g., Neuzil 1995, Saffer & Bekins 2006, Spinelli et al. 2006). In subduction zones, the geologic forcing is among the highest of any setting on Earth (Neuzil 1995). In combination with the low permeability typical of marine sediments, this leads to significant overpressures and to a dynamic and heterogeneous environment where active faulting is synchronous with rapid fluid expulsion. Thus the distribution of geologic forcing and permeability exert fundamental control on both pore pressure generation and the resulting flow pathways and rates; each of these is discussed in more detail below.

LFE: low-frequency earthquakes

Hydraulic conductivity (K): A geologic medium's capacity to transmit a particular fluid, measured in units of L/T; related to permeability through fluid viscosity and density

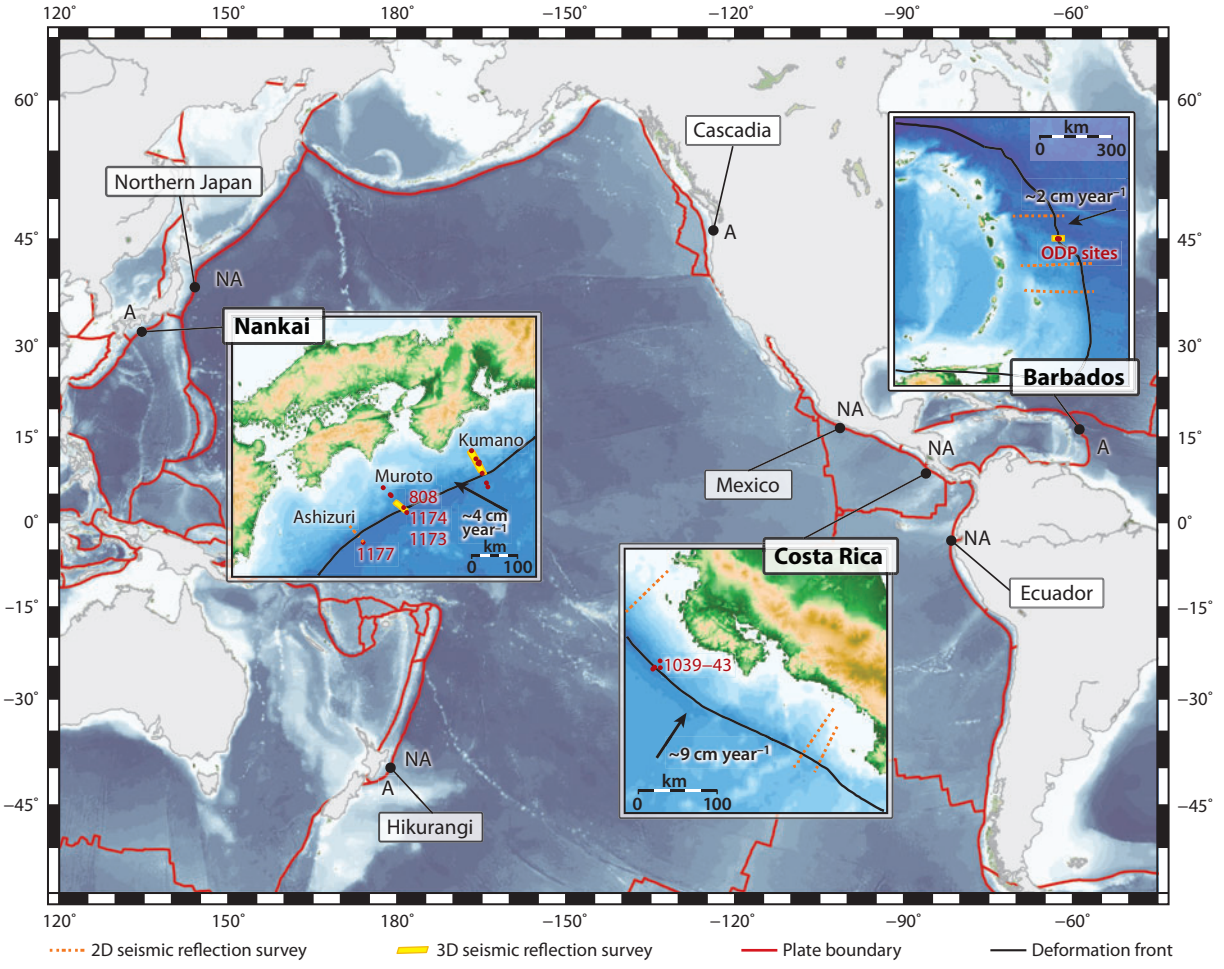

Figure 1

Locations of subduction margins discussed in this review, labeled as either accretionary (A) or nonaccretionary (erosive) (NA). Inset maps show details of three margins where sustained research focus has resulted in unusually rich and integrated offshore data sets. Numbered red dots mark Ocean Drilling Program (ODP) and Integrated Ocean Drilling Program (IODP) boreholes; orange dashed lines and yellow boxes show 2D and 3D seismic reflection surveys, respectively. On location map and insets, greater bathymetric depth is indicated by darker shades of blue. On inset maps, topography is shown, with green and brown indicating lower and higher elevation above sea level, respectively. The work of Hensen et al. (2004), Ranero et al. (2008), and Sahling et al. (2008) discussed in the text and shown in **Figure 6** is based on the seismic reflection profiles and seafloor mapping of the region shown in the Costa Rica inset. The Barbados inset shows locations of the seismic lines discussed by Bangs et al. (1990), along with the 3D survey described by Shipley et al. (1994) and Bangs et al. (1999) and shown in **Figure 4**. Research in the Nankai area has focused on three transects; the recent seismic reflection work described by Bangs et al. (2009) and Park et al. (2002, 2010) is from the Kumano transect.

2.1. Geologic Setting and Architecture of Subduction Zones

Approximately half of Earth's subduction zones are accretionary, and half are nonaccretionary (von Huene & Scholl 1991). At accretionary subduction zones, a portion of the fluid-rich sediment on the incoming oceanic plate is offscraped onto the leading edge of the overriding plate to build a tectonic wedge of sediment, and the remainder is carried beneath this wedge with the subducting plate (e.g., Davis et al. 1983). Additional sediment or rock may be transferred from the subducting

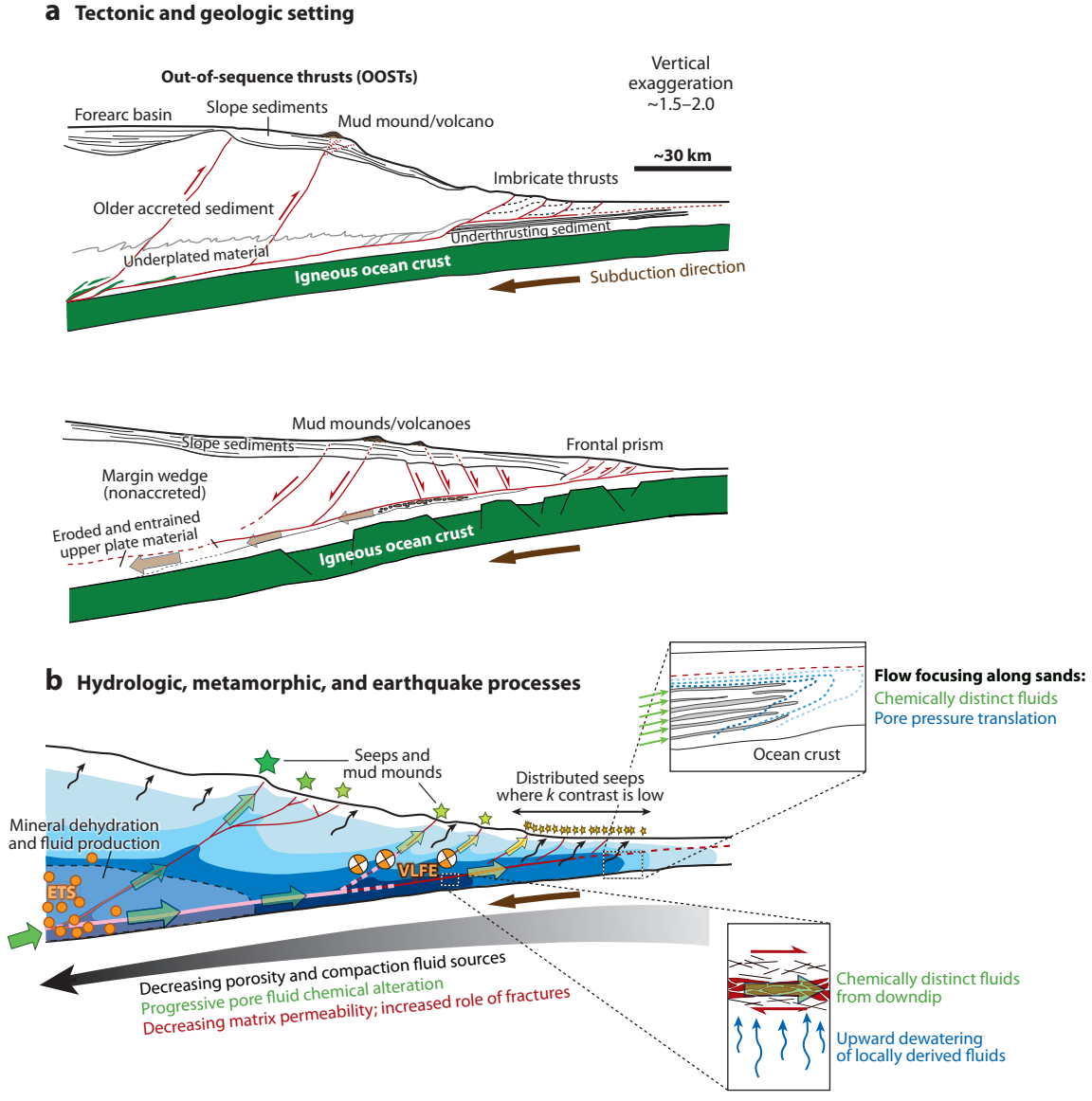

Figure 2

(*a*) Schematic cross sections showing tectonic and geologic elements of accretionary (*top*) and nonaccretionary (*bottom*) subduction zone forearcs. (*b*) Conceptual diagram summarizing several key hydrologic and fault slip processes. Blue shading denotes excess pore pressure, which affects the absolute strength of faults and sediments. Whether elevated pore pressures are localized within fault zones or are pervasive throughout the entire forearc is not well known. Arrows show fluid flow and are scaled qualitatively to illustrate flow rates; coloring of arrows represents the contribution of chemically distinct fluids produced by dehydration reactions, ranging from green (most distinct) to yellow (seawater composition). Flow along faults is likely mixed with locally derived fluids from dewatering of underthrust sediments. The igneous ocean crust may also host significant fluid flow that advects heat and/or solutes (not shown). Heavy pink lines illustrate the extent of coseismic slip (*solid*) and transitional zones at its updip and downdip edges (*dashed*). Very low-frequency earthquakes (VLFE) and episodic tremor and slip (ETS) occur at or near the updip and downdip limits of interseismic locking and coseismic slip, and their occurrence may be related to excess pore pressure that causes low effective stress (e.g., Ito & Obara 2006, Liu & Rice 2007). Insets show flow focusing and pressure translation along permeable sands (Underwood 2007) and within fractured fault zones that are permeable along but not across the shearing direction. Abbreviation: *k*, permeability.

to the overriding plate through underplating (**Figure 2*a***). The zone of active accretion near the trench is typified by imbricate thrusts that build the wedge, which thickens landward through a combination of movement on these faults, smaller-scale faulting, and diffuse thickening caused by lateral compaction and dewatering of the accreted sediment (Morgan & Karig 1993). Farther landward, the wedge thickens primarily through underplating, through pervasive deformation and slip on small-scale faults, and by slip on out-of-sequence thrusts (OOSTs).

OOSTs: out-of-sequence thrusts

Décollement: a low-angle detachment fault that acts as the main plate boundary in the outer forearc, which separates the overriding plate wedge from underthrusting sediments

Pore water: water contained in the intergranular space and fractures in sediment and rock

Bound water: water contained in the structure of hydrous minerals, and which is released during dehydration reactions

At nonaccretionary subduction zones, the leading edge of the overriding plate is an extension of onshore geology, and the sediment on the incoming plate is completely underthrust at the trench. In some cases, a small (~10-km wide) wedge is formed from recycled and accreted slope sediment (Kimura et al. 1997). At many of these margins, the upper plate is eroded at its base through tectonic processes and is characterized by subsidence and normal faulting (**Figure 2*b***) (e.g., von Huene & Scholl 1991). At both margin types, the décollement zone separates the underthrusting section from the overriding wedge, and researchers have imaged numerous major faults that cut the margin wedge and sole into the décollement, and that may act as permeable conduits for fluid escape (**Figure 2**). At accretionary margins, fluids are expelled both from the subducting plate sediments and igneous crust and from the compacting sediments incorporated into the accreting wedge. In contrast, at nonaccretionary margins, fluid expulsion originates only from the underthrusting sediments and subducting igneous crust; the hanging wall does not undergo significant dewatering.

2.2. Fluid Sources: Drivers of Pressure and Flow

Fluids entering subduction zones on the incoming plate include (*a*) pore water contained in intergranular and fracture porosity in the sediments and igneous crust, and (*b*) bound water within hydrous minerals, which is liberated by dehydration reactions. Geologic forcing in the outermost forearc is dominated by disequilibrium compaction associated with rapid burial and lateral

Figure 3

Example of fluid production and permeability distributions for the Ashizuri transect in the Nankai Trough (location shown in **Figure 1**). (*a*) Cross section showing temperatures computed from a thermal model and the locations of low-temperature diagenetic and metamorphic zones. (*b*) Distribution of fluid release from underthrusting sediments, reported in units of $Vol_{H2O}/Vol_{sediment}$ s^{-1}. Compaction-derived fluids are largest in the outer ~20–30 km of the forearc, beyond which clay transformation becomes increasingly significant. Deeper fluid production coincides with the transition from zeolite facies to prehnite-pumpellyite facies. Clay sources are computed following Saffer et al. (2008); deeper fluid release is based on stage-heating experiments of Bailey et al. (1964) and the thermal structure shown in panel *a*. (*c*) Summary of permeability for mudstone matrix and fault zones, based on laboratory and field measurements and the results of inverse modeling studies (*gray shaded regions*). In general, the permeability of faults is substantially higher than that of the matrix. The permeabilities shown here are based on effective stress-permeability relationships measured in the laboratory and field and on the assumption of a pore pressure ratio (λ) of 0.85 to define effective stress with distance from the trench. Permeability values for fault zones at the Barbados, Costa Rica, and Cascadia margins are also shown for comparison. References are as follows: 1, Screaton et al. 1995; 2, Skarbek & Saffer 2009; 3, Fisher & Zwart 1996; 4, Bekins et al. 1995; 5, Spinelli et al. 2006; 6, Saffer & Bekins 1998; 7, Kato et al. 2004; 8, Gamage & Screaton 2006. Open circles and triangles denote flow-through measurements; closed circles denote permeabilities derived from consolidation tests. Estimates of transient fault zone permeability (discussed in text; not shown) range from 10^{-13} to 10^{-11} m^2. Sediment permeability decreases monotonically with burial, whereas fluid sources do not, because dehydration peaks in specific pressure-temperature (P-T) windows. As a result, dehydration may release fluids into sediments characterized by low permeability, porosity, and compressibility, with significant effects on pore fluid pressure and geochemistry.

tectonic loading (**Figure 3*a*,*b***). The rate of compaction-driven dewatering decreases with progressive porosity loss owing to increasing sediment stiffness, and thus these fluid sources are generally largest within the first ~3–7 km of burial (Bekins & Dreiss 1992, Bray & Karig 1985) (**Figure 3**), with loading rates and corresponding fluid source terms up to ~10 times larger than those in even the most rapidly depositing sedimentary basins (e.g., Moore & Vrolijk 1992, Neuzil 1995). The distribution of compaction-driven fluid sources is typically estimated by (*a*) combining compilations of porosity data from active and exhumed subduction zones with computed trajectories for accreted and underthrust sediments as they are incorporated into the subduction complex (e.g., Bekins & Dreiss 1992, Screaton et al. 1990, Wang 1994), or (*b*) using constraints on sediment consolidation behavior that are obtained from laboratory experiments or borehole data, or that

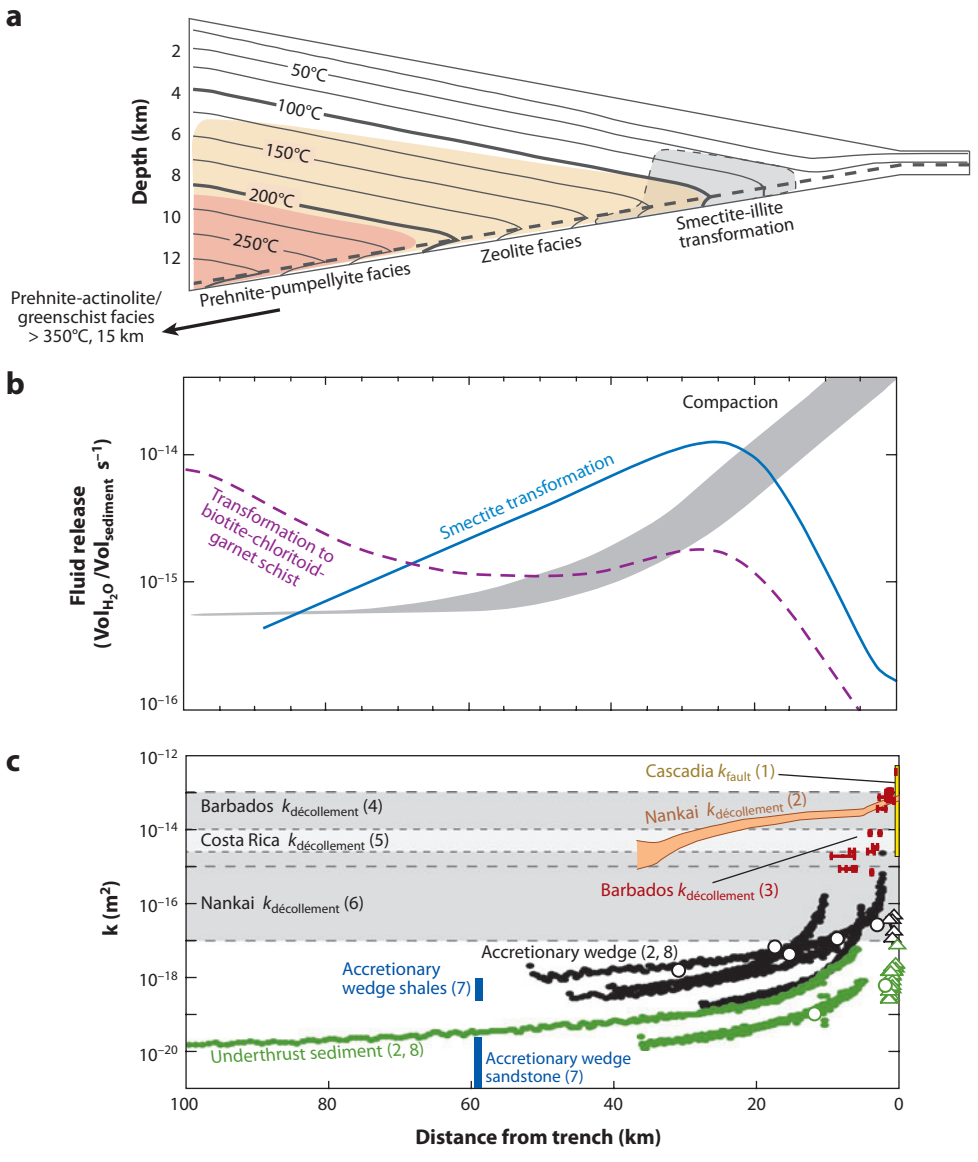

are inferred from seismic interval velocities (e.g., Calahorrano et al. 2008, Cochrane et al. 1994, Screaton et al. 2002) and incorporating these data into coupled numerical models of loading and consolidation (e.g., Gamage & Screaton 2006).

As sediments are exposed to increasing temperatures and pressures, fluid sources from dehydration overtake those from compaction. The fluids derived from sediment compaction in the outer forearc generally have a chemical composition similar to seawater, whereas fluids released by dehydration are freshened with respect to seawater and often characterized by elevated B and Li concentrations, thermogenic hydrocarbons, and distinctive $\delta^{37}Cl$, $\delta^{11}B$, $\delta^{18}O$, and δD signatures (e.g., Deyhle et al. 2003, Hensen et al. 2004, Kastner et al. 1991, Morris et al. 2003, Ransom et al. 1995). As discussed in Section 3.1, the observation of pore fluids with these chemical signatures in shallow boreholes and at vent sites provides some of the primary evidence for long-distance migration of dehydration-derived fluids along permeable stratigraphic and fault conduits (e.g., Kastner et al. 1991, Sahling et al. 2008, Tryon et al. 2010) (**Figure 2*b***).

At temperatures of ~60–150°C, clay dehydration and, to a lesser extent, opal dehydration and hydrocarbon generation become significant sources of fluid and likely contribute to overpressure development (e.g., Bekins et al. 1994, Bethke 1986, Bruce 1984, Spinelli & Saffer 2004). Fluid release from sediments at greater depths and temperatures accompanies the transitions from shale to chloritoid schist at temperatures of 100–225°C and to biotite-chloritoid-garnet schist at 225–~300°C (Bailey et al. 1964, Fyfe et al. 1978, Kerrick & Connolly 2001a). Pore collapse within basalt at temperatures of ~200–400°C is thought to release additional fluids, and dehydration of zeolite to greenschist facies minerals (mainly formed by hydration at the mid-ocean ridge and on the ridge flanks) liberates water at temperatures above ~400°C (Hacker 2008, Hacker et al. 2003, Kerrick & Connolly 2001b, Peacock & Hyndman 1999). Pore collapse and dehydration generally release fluids from the igneous crust below 20–30 km and farther than 120–150 km from the trench, excepting low-temperature dehydration of any clay minerals formed by alteration at the ridge. However, the released fluids may migrate updip or into the overlying forearc crust (**Figure 2*b***), where they can remain present as a free fluid phase or be consumed by retrograde (hydration) reactions (Peacock 2009). Breakdown of organic matter and decarbonation of limestone may produce CO_2 as an additional fluid source term, but these reactions are not expected to occur until depths of ~85–100 km, and computations based on realistic marine sediment compositions suggest that the mass of CO_2 released is only ~3% of that for H_2O (Gorman et al. 2006, Kerrick & Connolly 2001a).

For most common dehydration reactions, grain reorganization and recrystallization probably transfer much of the lithostatic load to the newly expelled fluid phase, as documented by both synmetamorphic veining and modeling studies that suggest that devolatilization occurs under conditions of severe fluid overpressure (Connolly 2010). Thus the geologic forcing (Γ) is commonly assumed to equal the total volume of fluid generated, reflecting the release of bound fluid and subsequent compaction of the rock (e.g., Bekins et al. 1995, Hanson 1992, Neuzil 1995, Wong et al. 1997). In general, kinetic effects and heterogeneity in the composition of fluid and solid phases in natural systems result in distributed fluid generation over a given temperature range, rather than in discrete "pulses" (**Figure 3*b***) (e.g., Kerrick & Connolly 2001a,b).

The largest dehydration-driven fluid source is from the transformation of smectite to illite (Bethke 1986). In mudstones typical of deep-water pelagic and hemipelagic environments, the total smectite abundance in the bulk sediment may be as high as ~45–50 wt% (Underwood 2007), corresponding to 8–10 wt% water (~15–20 volume %). The reaction is strongly controlled by kinetics and thus depends on both temperature and exposure time (e.g., Pytte & Reynolds 1988). Several detailed studies have quantified the magnitude and distribution of fluid sources from clay dehydration at individual margins by combining kinetic expressions with thermal

models and estimates of underthrust and accreted sediment trajectories (e.g., Bekins et al. 1994, Saffer et al. 2008, Spinelli & Saffer 2004) (**Figure 3*b***). These studies have shown that, depending on the initial sediment composition and thermal structure of the subduction zone, fluid sources from clay dehydration are comparable to, or exceed, those from compaction by ~10–40 km from the trench. Although less extensively investigated in subduction zones, hydrocarbon generation may also contribute to geologic forcing at temperatures of 60–150°C. Dissolved methane and higher-order hydrocarbons have been documented in pore waters at shallow depths (e.g., Morris et al. 2003) and in fluid inclusions sampled from exhumed subduction complexes, suggesting that these may comprise ~1–5 mol% of the fluid (Moore & Vrolijk 1992, Rowe et al. 2009).

Although several recent studies have quantified the distribution of H_2O and CO_2 release from metapelites, carbonate oozes, and hydrated igneous ocean crust at temperatures of ~300°C and higher (Connolly 2010; Hacker 2008; Kerrick & Connolly 2001a,b), fluid release from dehydration reactions in the temperature range ~150–300°C is not as well characterized because low-grade metamorphic minerals remain stable over a wide range of pressures and temperatures, and because the reaction kinetics are not as well known as for clay dehydration (e.g., Underwood et al. 1993). Estimates of fluid release have been obtained through stage-heating experiments and through characterization of the composition and volatile content of low-grade metamorphic assemblages that have well-constrained P-T histories (e.g., Bailey et al. 1964, Frey & Robinson 1999, Fyfe et al. 1978). These data suggest that fluid sources from dehydration significantly exceed those from compaction in this P-T range (**Figure 3*b***). Because this range of conditions coincides with the interseismically locked portion of the plate boundary along many subduction margins, the distributions of fluid release and pore pressure are of considerable interest (e.g., Oleskevich et al. 1999, Ranero et al. 2008).

Variations in sediment composition and clay content, thermal state, and hydration state of igneous crust from one margin to the next and along strike of individual margins (Underwood 2007) all play a key role in determining the inventory of pore and bound fluids; the distribution of their release; and their mechanical, geochemical, and hydrologic effects (e.g., Hacker 2008; Kerrick & Connolly 2001a,b). For example, in cold subduction zones, the effects of dehydration-derived fluids on both pore pressure and pore fluid geochemistry are amplified because porosity and sediment compressibility are low at the onset of dehydration, whereas in warm subduction zones, the dehydration-derived fluids are expelled and mixed into a larger pore space (e.g., Moore & Vrolijk 1992, Saffer & Bekins 1998). Ultimately, detailed characterization of individual margins through seafloor mapping and sampling, analysis of core samples, thermal modeling, and kinetic models of low-temperature dehydration are needed to quantify fluid source distributions (**Figure 3**) and to elucidate links between dehydration reactions; fluid pressure, flow, and chemistry (Hensen et al. 2004, Sahling et al. 2008, Teichert et al. 2005, Torres et al. 2004); and fault mechanical behaviors (e.g., Peacock 2009, Ranero et al. 2008, Schwartz & DeShon 2007, Spinelli & Saffer 2004, Wada et al. 2008).

2.3. Permeability: A Primary Control on Flow Rates and Pathways

In subduction zones, the high permeability of fractures, fault zones, and sandy strata is a primary control on drainage patterns and flow rates (Carson & Screaton 1998, Moore 1989), whereas the low permeability of compacting sediments limits the ability of fluids to access permeable conduits and facilitates the development of overpressures (e.g., Neuzil 1995, Saffer & Bekins 2002). Permeability anisotropy resulting from preferred grain orientation at small scales and sedimentary layering at the formation scale may also guide fluid flow and affect pore pressure.

However, laboratory measurements on shales show that permeability anisotropy developed during burial and consolidation is less than a factor of ~10 (e.g., Kwon et al. 2004), and modeling studies exploring the effects of regional permeability anisotropy caused by sedimentary layering illustrate that it can impact drainage efficiency and flow rates, but its importance is secondary to the absolute magnitude of permeability (Henry & Wang 1991, Saffer 2010).

Recent laboratory studies have provided new measurements of marine sediment permeability over a wide range of porosities and stresses, using core samples obtained from ocean drilling at several margins (Gamage & Screaton 2006, Saffer & McKiernan 2005, Zwart et al. 1997) (**Figure 3*c***). These studies show that permeability varies systematically as a function of lithology, and even the permeability of lithologically similar mud- and claystones decreases by 3–4 orders of magnitude, from $\sim 10^{-16}$ m^2 to $< \sim 10^{-20}$ m^2, as porosity is reduced from ~50% near the trench to <10% by 20–40 km landward. Recent work has also quantified fault zone permeability in active subduction zones, yielding values of fault-parallel permeability that are consistently 2–4 orders of magnitude higher than the sediment matrix (**Figure 3*c***). For example, direct measurements in shallow boreholes ($< \sim 1$ km) that sample active fault zones at the Barbados and Cascadia subduction zones document permeabilities of $\sim 10^{-13}$ to 10^{-15} m^2 and show that these permeabilities decrease strongly as a function of effective stress (e.g., Bekins et al. 2011, Fisher & Zwart 1996, Screaton et al. 1995, Screaton et al. 2000). Values obtained from detailed modeling studies of the Costa Rica, Nankai, and Barbados margins are in good agreement with the direct measurements, and they indicate time-averaged fault-parallel permeabilities of $\sim 10^{-13}$ to 10^{-17} m^2 (e.g., Bekins et al. 1995, Saffer & Bekins 1998, Skarbek & Saffer 2009, Spinelli et al. 2006).

High fault zone permeability is also inferred qualitatively from patterns of observed dewatering within subducting sediments that indicate upward drainage to a highly permeable décollement or fractured overriding wedge (Saffer 2003, Screaton et al. 2002) and from the observation of localized fluid seeps at and near faults at the seafloor (e.g., Henry et al. 2002). Fault zone architecture and the geometries and distributions of veins in exhumed fault systems provide further indirect evidence for enhanced fault permeability that is synchronous with fault activity (Fisher et al. 1995, Kondo et al. 2005, Labaume et al. 1997, Rowe et al. 2009). Observations from exhumed subduction thrust faults—including the Uganik thrust in Kodiak, Alaska (Rowe et al. 2009), and the Nobeoka thrust in the Shimanto Complex in southwestern Japan (Kondo et al. 2005)—also document that vein distribution and damage zone thickness are considerably thicker in the footwall than in the hanging wall, suggesting that the narrow active shear zone may act as an effective barrier to flow, whereas the adjacent damage zone acts as a conduit. This is consistent with laboratory measurements that document a permeability reduction of 3 orders of magnitude or more in sheared mudstones and clays (Brown et al. 1994, Ikari et al. 2009), and with observations of fault zone structure in active décollements (Tobin et al. 2001).

As shown in **Figure 3*c***, the contrast in permeability between matrix and fault zones increases with depth as compaction and cementation lead to reduced sediment permeability, with the result that fractures and fault zones probably become an increasingly important path for fluids with depth and distance from the trench (e.g., Moore 1989). Transiently elevated fault zone permeability is also suggested by (*a*) theoretical arguments demonstrating that the sensitivity of permeability to effective stress can give rise to solitary pressure waves (e.g., Bourlange & Henry 2007, Henry 2000, Rice 1992), (*b*) modeling studies showing that rapid transient fluid flow is needed to match observed seafloor flow rates and pore water geochemical signatures in shallow boreholes (e.g., Bekins et al. 1995, Saffer & Bekins 1998, Spinelli et al. 2006), (*c*) crack-seal textures in veins (e.g., Fisher et al. 1995), and (*d*) direct monitoring of fluid flow rate and geochemical variations that correlate with slip events (Solomon et al. 2009).

3. FLUIDS IN MOTION: PATHWAYS, RATES, AND THE NATURE OF FLOW

3.1. Fluid Budgets and Pathways

Fluids entering subduction zones with the incoming plate exit the system via diffuse flow at the seafloor, along structural or stratigraphic conduits, or are carried to greater depths beyond the forearc where their release influences a range of processes including mantle serpentinization, viscosity and flow, and magma generation and potentially triggers intermediate and deep earthquakes (e.g., Peacock 2009, Peacock & Hyndman 1999, Wada et al. 2008). Several recent studies have systematically inventoried fluid escape across forearcs through drilling, shallow coring, and seafloor surveys, and they have documented and quantified fluid fluxes across the seafloor from the trench to ~60 km landward (e.g., **Figure 2*b***) (Hensen et al. 2004, Sahling et al. 2008, Teichert et al. 2005, Torres et al. 2004, Tryon et al. 2010). In the wake of these new data, the partitioning of fluid expulsion from the forearc between focused discharge along fault zones and diffuse flow has emerged as a topic of significant interest. In particular, the importance of splay faults and OOSTs as pathways for fluid and solute transport has become increasingly appreciated (e.g., Ranero et al. 2008).

A diverse and extensive set of observations indicates qualitatively that localized fluid flow along permeable faults constitutes an important component of the fluid budget, and that it advects solutes and heat over distances of tens of kilometers (**Figure 2*b***). Flow rates at zones of focused fluid discharge range from a few millimeters per year to >200 m year^{-1}, as determined from seepage measurements at the seafloor (e.g., Henry et al. 2002, Linke et al. 1994), modeling of geochemical and thermal profiles (e.g., Hensen et al. 2004), and analyses of variations in the gas hydrate bottom simulating reflector (BSR) that indicate local warming associated with focused fluid upflow along thrust faults (e.g., Zwart et al. 1996). In contrast, diffuse flow rates range from ~0.4 to 40 mm year^{-1}, based on seafloor seepage measurements, analysis of heat flow data, and computed sediment dewatering rates (e.g., Bekins & Dreiss 1992, Brown et al. 2005, Davis et al. 1990).

Focused flow of chemically distinct fluids carrying the signature of dehydration reactions is documented by pore water geochemical and thermal anomalies centered at faults in boreholes (e.g., Bekins et al. 1995, Fisher & Hounslow 1990, Morris et al. 2003), by seeps and biological communities that correlate with faults and outcrops of permeable strata (e.g., Henry et al. 2002, Hensen et al. 2004, Sahling et al. 2008), and in the geological record by veins associated with fault zones, which in some cases contain low-salinity fluid inclusions that suggest transport of dehydration-derived fluids (e.g., Fisher et al. 1995, Kondo et al. 2005, Rowe et al. 2009). Geochemical analyses of venting fluids from mud mounds associated with faults cutting the margin wedge along the Costa Rica margin and of pore waters associated with fault zones in boreholes on the upper continental slope of the northern Japan margin have documented strong signatures of deeply sourced fluids, including marked pore water freshening, the presence of thermogenic hydrocarbons, elevated B concentrations, and $\delta^{18}O$ and δD values indicative of a high-temperature (80–120°C) source, highlighting the role of these structural features in tapping directly into zones of dehydration reactions within the underthrusting sediment (Hensen et al. 2004, Kopf et al. 2003). Seafloor mapping of vents has also raised the possibility that fracturing of the upper plate by subducting seamounts generates permeable pathways for deeply sourced fluids (Sahling et al. 2008).

In comparison with fluids sampled on the upper continental slope, those sampled from the décollement near the trench exhibit weaker geochemical signals of a deeply sourced component, including lower B and thermogenic methane concentrations and decreased pore water freshening (e.g., Hensen & Wallmann 2005, Morris et al. 2003). Similarly, in a transect of shallow boreholes across the outer 30 km of the Cascadia accretionary wedge offshore of Oregon, Teichert

et al. (2005) documented a pattern in which the proportion of dehydration-derived fluids increases systematically with distance landward from the trench. Taken together, these observations suggest that distinctive geochemical signatures from dehydration and water-rock reactions are diluted along flow paths to the seafloor because of mixing with local fluids derived from compaction, and that they will be strongest on the upper continental slope where permeable structures efficiently transport fluids from zones of dehydration (shown schematically in **Figure 2*b***). At nonaccretionary margins such as Costa Rica and northern Japan, the relative contribution of deeply sourced fluids at vents on the upper slope should be larger than that at accretionary margins because there is little or no compactive dewatering in the upper plate (e.g., Kopf et al. 2003, Ranero et al. 2008). However, at both types of margins, fluids flowing along the décollement become mixed with those derived from compaction of underthrusting sediments, leading to a diminished geochemical signal from dehydration in boreholes or at seeps near the trench. Fluids carried within the permeable décollement may also leak upward into the overlying sediments near the trench where the overriding wedge is thin, as suggested on the basis of geochemical observations (e.g., Hensen & Wallmann 2005), numerical modeling studies (Saffer & Bekins 1999), and zones of high seismic reflection amplitude interpreted to reflect fluid charging of strata immediately above the décollement (Bangs et al. 1999).

Despite extensive observations of vent sites, only recently have sufficient data been available from borehole transects (e.g., Teichert et al. 2005) and from comprehensive seafloor surveys and shallow coring programs (e.g., Ranero et al. 2008, Sahling et al. 2008) to quantify the role of faults, and particularly splay faults and OOSTs, in the overall forearc fluid budget. Simplified calculations in which locally measured flow rates are extrapolated across the margin on the basis of an assumed seep distribution suggest that as much as 80–95% of expelled fluids exit in localized zones of high permeability (Orange & Breen 1992). More recent work by Ranero et al. (2008) and Sahling et al. (2008) suggests that focused venting on the upper slope of the Costa Rica margin accommodates at least 5% of the overall fluid budget and as much as ~90% of the fluids released by mineral (clay) dehydration. Recent numerical modeling studies motivated by these data have incorporated splay faults as permeable conduits and have illustrated that these features can effectively tap the plate boundary to carry fluids, solutes, and heat to the seafloor (**Figure 2**) and that they may capture and transport as much as ~40% of the total fluids in the incoming sediments (Lauer & Saffer 2010).

Recent studies have also highlighted the potential role of the permeable upper igneous ocean crust in transporting fluids, solutes, and heat updip to the trench (e.g., Solomon et al. 2009, Spinelli & Wang 2008). For example, the numerical modeling studies of Matmon & Bekins (2006) and Spinelli et al. (2006) show that the igneous basement may serve as an important drainage pathway if it is hydrologically connected to the underthrusting sediments, especially if the underthrusting sediments are thin. This is consistent with the findings of Solomon et al. (2009), who argue that the geochemistry of basement pore fluids sampled at the Costa Rica margin reflects a contribution from underthrusting sediment. However, porosity data and inferred pore pressures within underthrusting sediments at several subduction zones show no indication of downward drainage (e.g., Saffer 2003, Saito & Goldberg 2001). Reconciling these conflicting observations and quantifying the role of the igneous oceanic crust as a potential permeable conduit remain important unresolved questions.

The extent of along-strike flow and transport is also a key issue in considering the origin and pathways of escaping fluids and solutes. Most numerical modeling studies and analyses of geochemical and thermal data have assumed a 2D flow system perpendicular to the trench. Although a 2D approximation may often be justified because it captures the largest gradients in driving forces and rock and fluid properties, recent 3D modeling studies have begun to illustrate the potential importance of trench-parallel fluid flow, caused by along-strike differences in taper angle that

drive pore pressure gradients (Cutillo et al. 2003, Screaton & Ge 1997) or differences in thermal structure that affect fluid viscosity and thus hydraulic conductivity (Spinelli & Saffer 2007), ultimately guiding flow for tens of kilometers along strike. However, few studies have rigorously explored these effects; thus the three-dimensionality of the flow systems remains poorly known.

3.2. Spatial Heterogeneity, Transience, and Associated Timescales

Data from a variety of approaches suggest that active fluid flow and elevated permeability within subduction zone faults are both heterogeneous and transient (**Figure 4**) (e.g., Bekins & Screaton 2007, Carson & Screaton 1998). For example, mapping of seismic attributes along fault surfaces suggests heterogeneity in consolidation patterns and channelization of fluid flow (Bangs et al. 1999, Shipley et al. 1994). Field observations document localized seafloor vent sites rather than continuous seepage along fault traces (e.g., Hensen et al. 2004, Sahling et al. 2008). Consideration of the overall fluid budget also suggests that to maintain flow rates similar to those observed at seep sites, fluid flow must be (*a*) collected and focused along permeable zones that occupy a fraction of the fault surface, (*b*) transient, or (*c*) some combination of the two (**Figure 4**) (e.g., Bekins & Screaton 2007). Finally, theoretical arguments and experimental data sets suggest that if fault zone permeability occurs by dilation, it cannot be uniform spatially because this would lead to a condition of zero shear strength along the subduction interface and thus to collapse of the margin wedge (e.g., Brown et al. 1994).

Evidence for transience includes geochemical and temperature anomalies centered at fault zones, which have been interpreted to reflect transient updip flow of chemically or thermally distinct fluids associated with periods of elevated fault zone permeability and subsequent diffusion of the signals away from the fault (Bekins et al. 1995, Bekins & Screaton 2007, Fisher & Hounslow 1990, Kastner et al. 1991, Spinelli et al. 2006). Analyses and modeling of geochemical profiles from boreholes across the décollement zone at several margins suggests that these flow transients initiated tens of thousands to hundreds of thousands of years ago (**Figure 4*a***) (Bekins et al. 1995, Henry 2000, Spinelli et al. 2006). Crack-seal textures within veins in exhumed and active fault zones record repeated hydraulic fracturing and precipitation events, providing additional evidence for transience in pore pressure and fluid flow (e.g., Fisher et al. 1995, Labaume et al. 1997). Direct observations from a seafloor monitoring system (Circulation Obviation Retrofit Kit, known as a CORK) at the Costa Rica subduction zone document changes in fluid chemistry and abrupt increases in both fluid flow rate and pore pressure at the décollement that correlate with SSE on a much shorter timescale. These observations provide some of the first clear and direct evidence for temporally varying hydrologic processes within subduction zone faults (**Figure 5**) (Davis & Villinger 2006, Solomon et al. 2009).

The timescale of tens to hundreds of thousands of years estimated from geochemical and thermal anomalies is far greater than earthquake recurrence intervals or the timescale of hydrologic transience seen in CORK data. One possible explanation is that in addition to transient permeability variations associated with fault slip, there is a separate, longer-term hydrologic transience caused by the buildup and release of pore pressure that drives regional fluid flow events. Alternatively, the apparent timescale of transience estimated from geochemical profiles may simply document the initiation of flow localization and thus reflect the approximate time since fault formation (Saffer & Bekins 1999). This hypothesis is consistent with the fact that pore water geochemical profiles indicating transience are observed in boreholes near the trench, where the age of accretion, and thus of décollement formation, is comparable to the inferred timescale of flow initiation. In this scenario, fluid flow would be quasi-continuous from the time of fault initiation to the present (with transients associated with earthquakes superimposed on this pattern), and

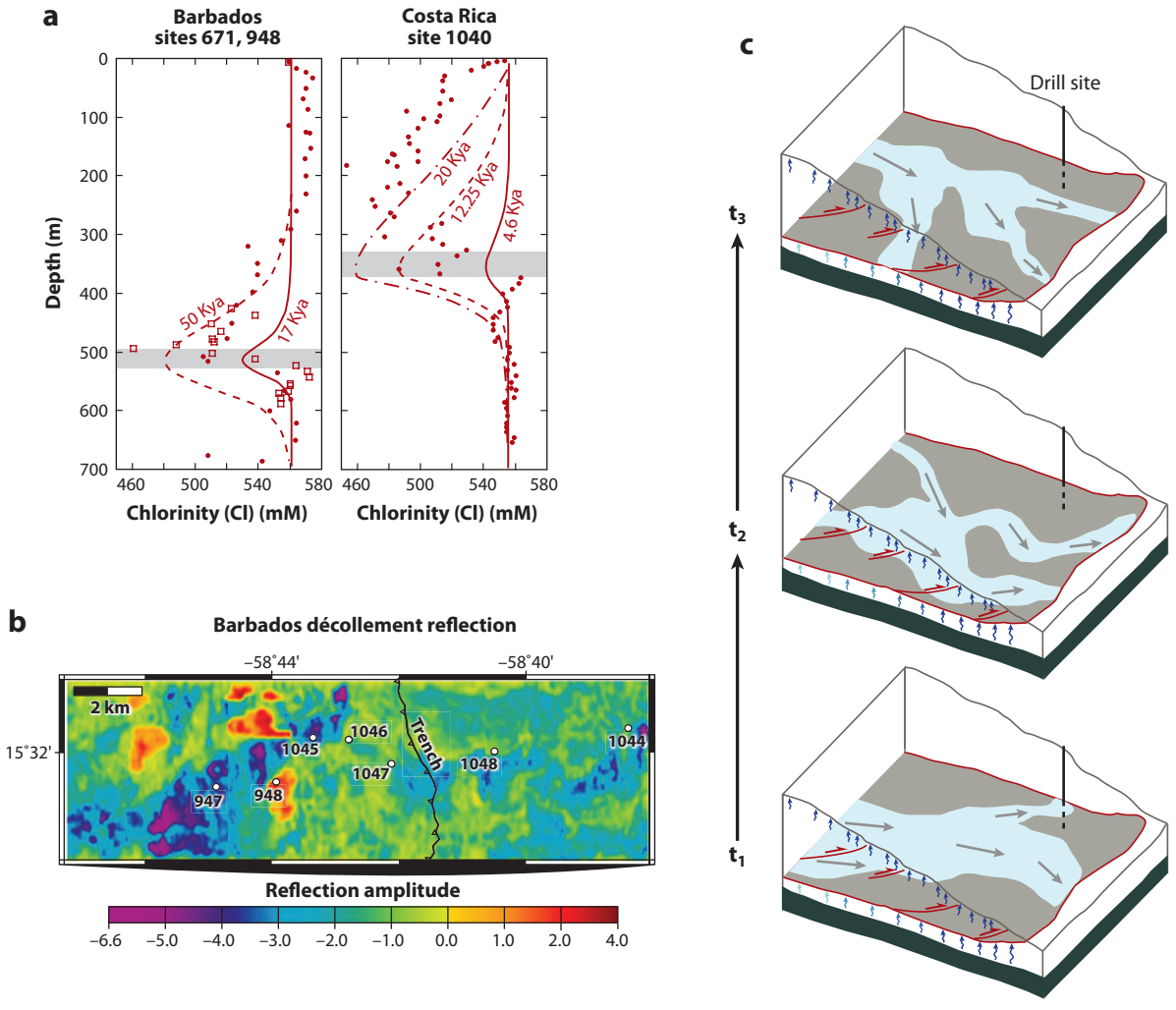

Figure 4

Summary of observations suggesting that fluid flow along faults is both transient and spatially heterogeneous. (*a*) Pore water chloride profiles for drill sites at the Barbados and Costa Rica margins, with modeling results that show the duration of transient flow along the décollement zone (*gray shaded zone in each plot*) needed to match observations. Barbados from Saffer & Bekins 1999; Costa Rica from Spinelli et al. 2006. (*b*) Seismic reflection amplitude of the décollement at the Barbados margin, showing a zone of strong negative polarity reflectivity (*blue and purple areas*), interpreted as a high-porosity and high-permeability "channel." After Shipley et al. 1994, Bangs et al. 1999. (*c*) Schematic diagram showing one way to reconcile observations that suggest both transient and heterogeneous focused flow along the décollement. Kya, thousands of years ago; t, time.

the timescale of the shifting conduits shown in **Figure 4*c*** would coincide with earthquake events. Although a substantial body of evidence from direct long-term monitoring (Brown et al. 2005, Davis et al. 2006, Davis & Villinger 2006, Solomon et al. 2009), geologic observations (e.g., Fisher et al. 1995, Shipley et al. 1994), and inferences from overall budget calculations (e.g., Bekins & Screaton 2007) argue clearly for transient and heterogeneous fluid flow along faults, its nature and timing remain incompletely understood, as do links between flow transients, pore pressure fluctuations, and fault slip.

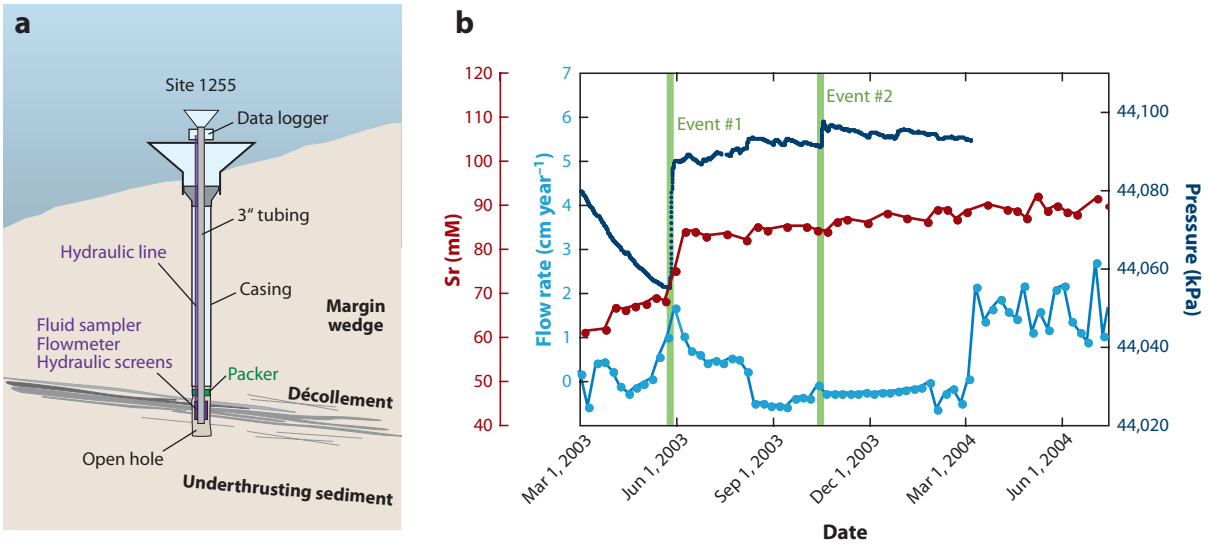

Figure 5

(*a*) Diagram of a Circulation Obviation Retrofit Kit (CORK) installation monitoring the décollement at Integrated Ocean Drilling Program (IODP) Site 1225 at the Costa Rica subduction zone. (*b*) Data from the installation showing fluctuations in fluid flow rate, pore water geochemistry, and pore pressure. Changes are temporally correlated with slow slip events documented by continuous global positioning system (GPS) stations on land (*green vertical lines*). Modified from Solomon et al. 2009 with permission from Elsevier.

4. TRAPPED FLUIDS: MECHANICAL EFFECTS OF ELEVATED PORE PRESSURE

Pore fluid pressure counteracts normal stress and ultimately exerts a direct control on mechanical responses, ranging from sediment compaction to the shear strength and sliding stability of tectonic faults (e.g., Davis et al. 1983, Hubbert & Rubey 1959, Scholz 1998):

$$\sigma_n' = \sigma_n - P_f \tag{2}$$

$$\tau = C + \sigma_n' * \mu, \tag{3}$$

where τ and σ_n are the shear and normal stresses acting on a plane, σ_n' is the corresponding effective normal stress, C is cohesion, μ is the coefficient of friction, and P_f is the fluid pressure. In particular, elevated pore pressure has been widely invoked as a mechanism to explain the apparent mechanical weakness of plate-boundary faults in a variety of tectonic settings (e.g., Davis et al. 1983, Rice 1992). The degree to which fluid pressure counteracts the total normal stress generated by the lithostatic load is commonly expressed in the form of the overpressure ratio (λ) or modified pore pressure ratio (λ^*):

$$\lambda = \frac{P_f}{P_l}; \quad \text{and,} \quad \lambda^* = \frac{(P_f - P_h)}{(P_l - P_h)}, \tag{4a,b}$$

where P_l is the lithostatic pressure and P_h is the hydrostatic pressure (see sidebar, Hydrostatic and Lithostatic Pressure). All three values (P_f, P_l, and P_h) are adjusted by subtracting the hydrostatic pressure associated with ocean depth.

HYDROSTATIC AND LITHOSTATIC PRESSURE

Hydrostatic pressure is the downward pressure exerted by a water column at a given depth through an open network of pores, equal to $\rho_f gz$, where ρ_f is fluid density and z is depth. Lithostatic pressure is the vertical stress generated by overlying rock and sediment (including pore fluids) at any given depth, equal to $\rho_b gz$, where ρ_b is the average rock bulk density.

4.1. Pore Pressure Quantification and Effects on Fault Strength

Qualitative indicators of elevated pore pressure in subduction zone forearcs are abundant and varied. These include extensional veining observed at depths ranging from a few hundred meters in active fault systems to >40-km depth in exhumed subduction complexes (e.g., Byrne & Fisher 1990, Labaume et al. 1997, Rowe et al. 2009), as well as active mud volcanism observed at many subduction margins, which manifest elevated pore pressures that drive fluids and mud from depths of >10 km (Kopf 2002). Mechanical analyses also predict that accretionary wedges and their basal décollements must be highly overpressured to explain active slip on shallowly dipping faults and the ubiquitously observed thinly tapered wedge geometry (e.g., Davis et al. 1983, Hubbert & Rubey 1959).

Recent work has made important strides in quantifying pore fluid pressure and its distribution using data and samples from boreholes and using seismic reflection data that extend observations from boreholes for tens of kilometers laterally and downdip. At the scale of individual boreholes, estimates of in situ effective stress are based on laboratory reconsolidation testing of core samples and analysis of porosity and P-wave velocity data (e.g., Moore & Tobin 1997, Saffer 2003, Screaton et al. 2002). Direct measurements of pore pressure have been obtained in a small number of sealed and instrumented boreholes (CORKs) and industry wells, but CORKs are limited to shallow depths in the outermost forearc (Becker et al. 1997, Davis et al. 2006), and industry wells are few and at shallow structural levels farther arcward (Sibson & Rowland 2003, Suppe 1981). Nonetheless, these studies document elevated pore pressures of $\lambda = \sim 0.65$–0.90 in the underthrusting sediments, décollement zone, and interior of accretionary wedges at several subduction margins.

Seismic reflection data have also been used to document pore fluid conditions from reflectivity and seismic velocity anomalies in and below major faults. These include high-amplitude, negative-polarity fault zone reflections, interpreted to indicate anomalous fluid content or fluid pressure within or subjacent to faults (e.g., Bangs et al. 1999, 2004, 2009; Moore et al. 1990; Park et al. 2002; Tobin et al. 1994), and zones of anomalously low P-wave velocity, interpreted to reflect regions of undercompaction related to poorly drained conditions and excess pore pressure (e.g., Bangs et al. 2009, Park et al. 2010). In some cases, these reflectivity and velocity anomalies have been speculatively linked to zones of elevated pore pressure, fluid release from dehydration reactions, and the updip terminus of seismic fault slip (Bangs et al. 2009; Park et al. 2002, 2010; Ranero et al. 2008). For example, at the Costa Rica margin, Ranero et al. (2008) note spatial correlations between the anticipated locations of mineral dehydration and elevated pore fluid pressure; high-amplitude, negative-polarity seismic reflectivity; surface seeps that have distinct geochemical signatures; and the limits of earthquake slip (**Figure 6**). The authors hypothesize that the reflectivity effectively maps fault zone fluid content associated with clay dehydration and that the fault becomes seismogenic where these fluid sources have dissipated and where the fault is comparatively less fluid rich (discussed further in the following section). Similar correlations are less evident at other well-studied margins: For example, along the Nankai margin, the location

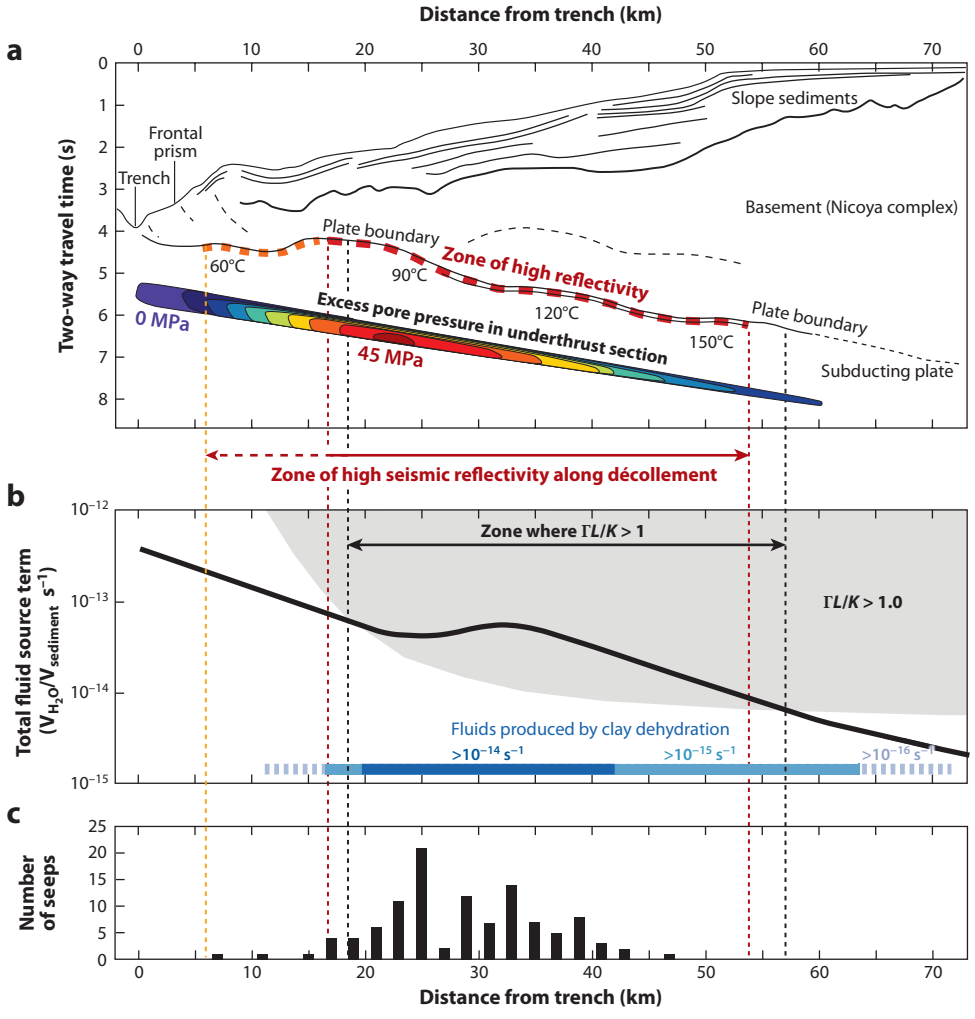

Figure 6

Compilation of observations and modeling results for the Costa Rica margin, illustrating the spatial relationships among (*a*) décollement zone reflection amplitude (Ranero et al. 2008) and excess pore pressure simulated in numerical modeling studies (Lauer & Saffer 2010); (*b*) fluid sources and zone of anticipated excess pore pressure based on the criterion of Neuzil (1995), together with modeled fluid generation from clay transformation (*blue bar shows fluid sources greater than* 10^{-14} s^{-1}, 10^{-15} s^{-1}, *and* 10^{-16} s^{-1}, *as noted*) (Spinelli & Saffer 2004); and (*c*) distribution of fluid seeps with sufficient methane flux to support chemosynthetic communities or to form mappable carbonate deposits at the seafloor (Sahling et al. 2008). It is postulated that the reduced seismic reflection amplitude ~55 km arcward of the trench maps decreased fluid content and pore pressure at the plate interface and that it marks the updip (shallow) extent of earthquake rupture (Ranero et al. 2008). Γ, magnitude of geologic forcing; *K*, hydraulic conductivity; *L*, drainage path length.

of a widespread high-amplitude seismic reflector is deeper and ~20 km farther arcward than the estimated locus of clay dehydration (Park et al. 2002). It is unclear whether this zone of enhanced reflectivity is related to other, deeper metamorphic reactions; to mechanical processes that affect the fault zone structure; or to lithologic or hydrologic contrasts across the fault related to sand bodies, cementation, or underplating of igneous ocean crust (e.g., Kato et al. 2004).

Constraints on pore fluid pressure within fault zones are particularly scarce. At the central Oregon margin, Tobin et al. (1994) linked seismic reflection waveform and amplitude modeling to laboratory measurements on core samples to quantify fluid pressure in the frontal thrust at a depth of 400–500 m below the wedge surface and found that significant overpressures ($\lambda^* = 0.86$–0.98) in the fault zone would be needed to explain the reflections. Similarly, Shipley et al. (1994) and Bangs et al. (1999) were able to quantitatively associate Barbados décollement reflectivity with data from boreholes, showing that very high porosities (~70%) are maintained in regions of the décollement, presumably owing to inhibited drainage (**Figure 4*b***). However, the presence of brittlely damaged fault rock offers an alternative explanation for low seismic impedance in fault zones, without the requirement for fluid pressure or trapped porosity, especially as wall rock becomes more lithified (Gettemy et al. 2004). Thus careful waveform analysis and petrophysical insight, ideally with core samples, are needed to confidently associate seismic reflection attributes with pore fluid conditions.

Although pore pressure, stress, and strength of the plate-interface décollement are central to the mechanics of faulting, direct measurement of these quantities has proven elusive. Thus several recent studies have focused on quantifying pore pressure in the upper underthrusting sediment, where pore pressure and compaction state are tightly linked to fault strength; these sediments lie immediately subjacent to the fault, lining the base of the wedge, and the décollement commonly steps downward into them (e.g., Byrne & Fisher 1990). Within underthrusting sediment, the stress state is assumed to follow a uniaxial burial path owing to vertical (gravitational) loading (e.g., Byrne & Fisher 1990). For this relatively simple stress and strain path, relationships between seismic velocity, porosity, and effective stress can be calibrated locally at basinal reference boreholes or estimated using global compilations. These relationships then allow quantification of in situ effective vertical stress and pore pressure from measured porosities in boreholes (e.g., Saffer 2003, Screaton et al. 2002) or from P-wave interval velocities derived from seismic reflection data (e.g., Calahorrano et al. 2008, Cochrane et al. 1994, Tobin & Saffer 2009) (**Figure 7**).

Borehole-based studies indicate that even within ~1–4 km of the trench, pore pressures within underthrusting sediment are typically more than 60–70% of the lithostatic load ($\lambda = 0.68$–0.97; $\lambda^* = 0.20$–0.91) (e.g., Becker et al. 1997, Saffer 2003, Screaton et al. 2002). Results from analyses of seismic reflection data show that these elevated pore fluid pressures extend to at least 20–30 km from the trench. For example, a recent study along the Muroto transect at the Nankai margin concludes that excess pore pressure is ~5 MPa by 2–3 km arcward of the trench and that it increases to ~9 MPa by 20 km (**Figure 7**), corresponding to $\lambda \geq \sim 0.75$ along the base of the wedge in the outer forearc (Tobin & Saffer 2009). A similarly detailed study of the Ecuador margin documents excess pore pressures of 8 to 40 MPa ($\lambda \geq 0.75$–0.8) from the trench to 25 km arcward (Calahorrano et al. 2008). These studies document that effective stress at both margins remains $<\sim$10 MPa, to 20 km from the trench. By Equation 3 and through assumption of a friction coefficient typical for marine sediments, this corresponds to a shear strength of only $<\sim$4 MPa along the wedge base, offering a quantifiable and plausible explanation for a mechanically weak subduction plate interface. Beyond ~20–30 km from the trench, both studies document a trend of decreasing porosity, increasing effective stress, and decreasing pore pressure ratio, all of which may be linked to downstepping of the décollement and to decreasing amplitude of the décollement seismic reflection (Bangs et al. 2004, Calahorrano et al. 2008).

In contrast, relatively few studies have estimated pore pressure above the décollement within accretionary or erosive wedges. Typically, the wedge is lithologically more diverse than the underthrust section, in that it contains more abundant turbidites and ashes. In addition, it has undergone a complex stress history, making pore pressure prediction difficult. Porosity and P-wave velocity vary strongly with both mean and differential stress (e.g., Karig 1990) and are also affected by diagenesis

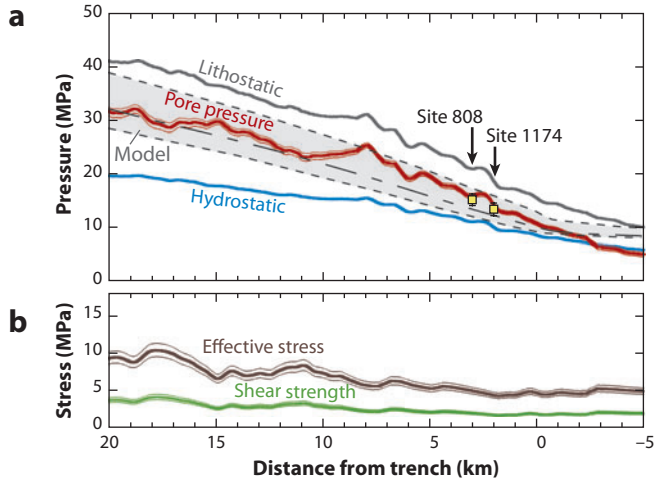

Figure 7

(*a*) Hydrostatic (*blue curve*), lithostatic (*gray curve*), and pore fluid pressure (*red curve*) computed from seismic interval velocities within underthrusting sediments in the Nankai Trough from the trench to 20 km landward of the trench (corresponding to a burial depth of ~2.5 km) (after Tobin & Saffer 2009). Calculated pore pressures are in good agreement with the results of independent hydrologic models (*gray region and dashed black lines*) and indicate poorly drained conditions, with $\lambda = \sim 0.75$. Pore pressures estimated from porosity data at boreholes are shown for comparison (*yellow squares*) (Screaton et al. 2002). (*b*) Effective stress (*brown*) and shear strength (*green*) defined from the values shown in panel *a* and assuming a friction coefficient of 0.4. Upper and lower bounds on pore pressure, effective stress, and shear strength (*fine lines*) reflect propagated uncertainties as described by Tobin & Saffer (2009). Upper and lower bounds on modeled pore pressures reflect the effect of increasing and decreasing sediment permeability in the model by a factor of 3. Effective stress remains <10 MPa beneath most of the outer forearc, and estimated shear strength of the décollement therefore remains <4 MPa.

(Gettemy & Tobin 2003), further confounding efforts to quantify pore pressure from compaction state or seismic interval velocity. Studies that nevertheless attempt to map seismic velocity and/or porosity to pore pressure in accretionary wedges have assumed a ratio of horizontal and vertical stresses linked to a particular rock failure criterion or constitutive soil model (e.g., Flemings 2002, Moore & Tobin 1997, Tsuji et al. 2008), or have employed the highly simplified assumption that a uniaxial burial curve can be applied to the wedge interior (e.g., Bangs et al. 1990, Westbrook 1991).

When viewed collectively, recent well-constrained quantifications of pore pressure from borehole data, reconsolidation tests, seismic interval velocities, and numerical modeling consistently illustrate that pore pressures reflect a dynamic balance between geologic forcing and fluid escape (**Figure 8**). These detailed studies also extend the analysis of Neuzil (1995) to show that the magnitude of excess pore pressure scales systematically with the ratio $\Gamma L/K$ (**Figure 8**). This pattern is consistent across several subduction margins, which span a wide range of permeability, subduction geometry, burial rate, and sediment thickness, suggesting a simple and useful framework for considering the underlying processes that govern excess pore pressure generation and maintenance. This conceptual model implies that margins characterized by thick and/or low-permeability incoming sediment should be poorly drained, leading to high pore pressure, low fault strength, and small taper angles (e.g., Barker et al. 2009, Saffer & Bekins 2002). In contrast, highly porous and permeable near-surface sediments are subducted at erosive margins, resulting in better-drained conditions associated with lower pore pressure, a strong plate interface, and a steeply tapered margin wedge (e.g., Barker et al. 2009, Lallemand et al. 1994).

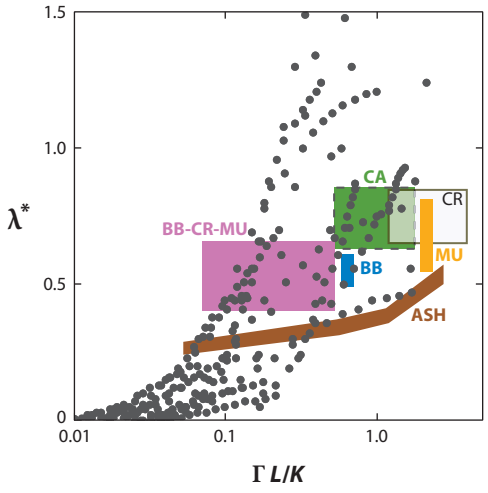

Figure 8

Compilation of numerical modeling results and pore pressure estimates, showing the systematic relationship between excess pore pressure and Neuzil's (1995) ratio of fluid sources, drainage path length, and hydraulic conductivity, computed following the approach of Saffer & Bekins (2006). CR, numerical modeling result from Costa Rica (Spinelli et al. 2006); MU, numerical modeling result and pore pressures computed from seismic reflection interval velocities for the Muroto transect in the Nankai Trough (cf. **Figure 7**) (Tobin & Saffer 2009); ASH, numerical modeling result for the Ashizuri transect (Saffer 2010); CA, numerical modeling results and pore pressures estimated from seismic reflection data for Cascadia (Wang 1994); BB, numerical modeling results and pore pressures estimated from seismic reflection data at Barbados (Bangs et al. 1990, Bekins et al. 1995); BB-CR-MU, pore pressures inferred from borehole porosity data at Barbados, at Costa Rica, and along the Muroto transect (Saffer 2003, Screaton et al. 2002). Gray circles show results of a generic parametric study from Saffer & Bekins (2006). λ^*, modified pore pressure ratio; Γ, magnitude of geologic forcing; K, hydraulic conductivity; L, drainage path length.

4.2. Role of Fluids in Fault Locking, Earthquakes, and Other Modes of Fault Slip

Elevated fluid pressure has been invoked as a possible explanation for a wide range of new and old seismological observations along subduction plate interfaces, including (*a*) inhibition of shallow seismicity (e.g., Scholz 1998); (*b*) promotion of a relatively deep and wide seismogenic zone (Fagereng & Ellis 2009); (*c*) facilitation of great earthquake propagation to the trench and enhanced tsunami strength (e.g., Dean et al. 2010); (*d*) inhibition of great earthquake propagation to the trench area (e.g., Park et al. 2002); and, recently, (*e*) facilitation of tectonic tremor, SSE, LFE, and VLFE (e.g., Ito & Obara 2006, Kao et al. 2005, Obana & Kodaira 2009). It is evident that elevated pore pressure is commonly invoked to explain even mutually contradictory phenomena; this is indicative of the incomplete state of knowledge about the relationship between pore pressure and modes of fault slip.

Seismogenic zone (specific to subduction zones): portion of the subduction plate boundary generally thought to accumulate sufficient elastic strain in the interseismic period to fail in earthquakes and radiate seismic energy

Within the forearc, including the seismogenic zone and its updip and downdip transitions, a variety of new modes of slip have been discovered through new geodetic and seismic techniques, blurring the boundary between seismic and aseismic fault mechanics (e.g., **Figure 2*b***). These observations include SSE (e.g., Song et al. 2009), LFE and VLFE (e.g., Ito & Obara 2006), and tectonic tremor with or without slow slip (also known as nonvolcanic tremor and ETS, respectively; e.g., Shelly et al. 2006). Hypotheses explaining these phenomena commonly associate them with elevated pore pressure and low effective normal stress, potentially related to the loci of

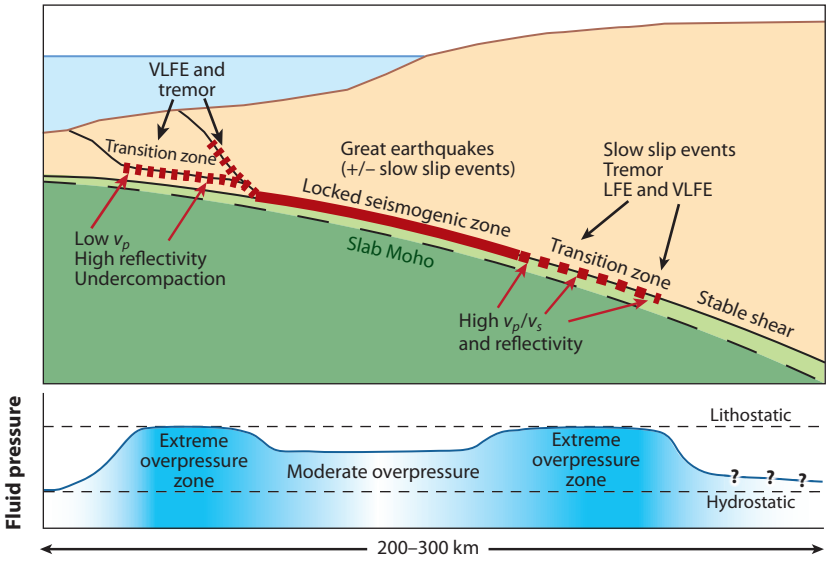

Figure 9

Conceptual diagram of fluid pressure distribution along the subduction interface and its relationship to frictional slip domains on the megathrust based on geophysical observations, mainly from the Nankai Trough, Cascadia, Ecuador, and southern Mexico (e.g., Audet et al. 2009, Kato et al. 2010, Obana & Kodaira 2009, Song et al. 2009, Tobin & Saffer 2009). The locked seismogenic patch may be overpressured, but perhaps not to lithostatic or near-lithostatic levels. The updip transition zone is marked by evidence for anomalous porosity, P-wave velocity, and reflectivity, as well as the occurrence of very low-frequency earthquakes (VLFE) and tectonic tremor, all suggesting elevated fluid pressure and extremely low effective stress. Near-lithostatic pore pressures in this region likely result from a combination of compaction disequilibrium and fluids released by clay dehydration (cf. **Figure 6**). The corresponding downdip transition zone is also marked by velocity and reflectivity anomalies, tectonic tremor, low-frequency earthquakes (LFE) and VLFE, and slow slip events, all hypothesized to indicate extreme pore fluid overpressure and thus low effective stress, potentially caused by fluid release through metamorphic dehydration reactions.

metamorphic dehydration reactions (**Figure 9**) (e.g., Gomberg 2010, Ito & Obara 2006, Obana & Kodaira 2009, Song et al. 2009). For example, Ide et al. (2007) examined these unusually slow deformation events collectively and suggest that very high pore fluid pressures likely facilitate the slip events, although it is not the only permissible cause. In numerical models of fault slip, Liu & Rice (2007) show that SSE arise in the downdip transition zone only under conditions of near-lithostatic pore fluid pressure. At the northern Hikurangi margin, Bell et al. (2010) found several zones of high-amplitude seismic reflections, interpreted as fluid-charged and overpressured sediments, at 5–15-km depth and spatially associated with known SSE. Recently, VLFE and tremor activity have also been detected in the outer accretionary prism of the Nankai Trough (Ito & Obara 2006, Obana & Kodaira 2009) and are characterized by anomalously low estimated stress drops of 0.1 to 6 kPa (compared with normal earthquake stress drops of 1 to 10 MPa). The authors argue that extremely high pore fluid pressure and low effective normal stress on fault planes would allow both the low stress drops and tremor behavior.

Independent evidence for such elevated pore fluid pressure comes in the form of unusually low seismic velocity and high Vp/Vs ratio (**Figure 9**). Recent work using seismic tomographic methods has shown for the Tokai region of Japan (Kato et al. 2010, Kodaira et al. 2004) and for southern Mexico (Song et al. 2009) that SSE are coincident with regions of low shear wave velocity

(Vs) and high Vp/Vs ratio in subducted oceanic crust, with shear wave velocity as much as 30–54% lower than for typical hydrated oceanic crust. All three studies conclude that this likely arises from a zone of high pore fluid pressure at 25–50-km depth and between the estimated locations of the 350–450°C isotherms. This zone is bracketed both updip (locked seismogenic zone) and downdip (ductile shear zone) by zones of higher velocity and inferred lower pore fluid pressure, suggesting that pore pressure is highest where the SSE occur. Under Vancouver Island, as Audet et al. (2009) also document, is a low-velocity zone corresponding to the locus of ETS.

At the updip end of the seismogenic plate interface, Calahorrano et al. (2008) and Tobin & Saffer (2009) found evidence that near-lithostatic pore pressure along the base of the forearc wedge begins to dissipate ~20–30 km landward of the trench (**Figure 7**). Similarly, Ranero et al. (2008) attribute the diminished amplitude of the negative-polarity plate-boundary seismic reflection at Costa Rica to decreasing fluid content and the onset of seismogenic locking. At both margins, numerical hydrologic modeling results also suggest that excess pore pressure dissipates at or near the updip edge of the seismogenic zone (e.g., Saffer & Bekins 1998, Spinelli & Saffer 2004, Spinelli et al. 2006) (**Figure 6**). The idea that reduced fluid pressure and increased effective stress may mark the onset of seismogenic locking is consistent with theoretical arguments showing that the tendency toward unstable slip increases with increased effective stress (Scholz 1998).

Taken together, these studies paint a picture of a subduction interface with shallow and deep aseismic or conditionally seismic zones that are at extreme (near-lithostatic) overpressure, and a seismogenic locked zone in between where pore pressure may be more modest and effective stress correspondingly higher (**Figure 9**). Whether this is true, universally or at any margin, remains to be determined. This view may be at odds with arguments based on earthquake stress drop (Magee & Zoback 1993) and on wedge geometry that the seismogenic portion of the plate boundary is weak because of high fluid overpressure. Alternatively, it may simply point to a conclusion that the fault system is overpressured everywhere but that it approaches the lithostatic limit only at the transitional ends of the seismogenic zone. Many uncertainties remain with respect to the role of fluid pressure in plate-boundary fault processes, and this will continue to be a major topic of research.

5. SUMMARY AND OUTSTANDING QUESTIONS

Through wide-ranging investigations that have included detailed multidisciplinary studies of individual margins, field measurements on and beneath the seafloor, laboratory studies that provide important new constraints on rock properties, and increasingly sophisticated numerical modeling, our knowledge of coupled hydrogeologic and tectonic processes at subduction zones has become both more comprehensive and quantitative than in previous decades. This improved understanding nevertheless highlights a number of key remaining unknowns. Chief among them are (*a*) the spatial and temporal variability of fault zone and sediment permeability and the underlying processes that govern the magnitude and timescales of transience; (*b*) the role of oceanic basement as a drainage path or conduit for heat and solute transport; (*c*) the distribution of fluid production, permeability, and pore pressure in the crucial zone between ~150° and ~350°C where seismogenic locking predominantly occurs; (*d*) quantitative links between remotely sensed geophysical properties (such as the Vp/Vs ratio or reflectivity) and in situ hydrogeologic conditions; and (*e*) the hypothesized role of fluid pressure in governing newly observed modes of fault slip. The interdependence of tectonic deformation and hydrogeologic processes at all spatial and temporal scales dictates that significant advances will likely require tightly integrated and interdisciplinary approaches, as exemplified by some of the recent studies highlighted here.

SUMMARY POINTS

1. Sediment permeability decreases monotonically with burial, whereas fluid sources do not, because dehydration peaks in specific P-T windows. As a result, dehydration releases fluids into sediments characterized by low permeability, porosity, and compressibility, with profound effects on pore fluid pressure and geochemistry.
2. Faults play an important role in the overall hydrologic budget of forearcs, and localized flow along them probably becomes increasingly significant with depth and distance from the trench as the sediment matrix permeability is decreased by consolidation and cementation. Splay faults and OOSTs that cut the margin wedge appear to tap zones of mineral dehydration, and transport fluids and solutes efficiently from the plate interface and underthrusting plate to the seafloor.
3. Several lines of evidence indicate that fluid flow in permeable fault zones is both transient and spatially heterogeneous. New time-series observations from CORKs provide important documentation that permeability and pore pressure changes are associated with fault slip events, yet other indicators suggest timescales of tens to hundreds of thousands of years for hydrologic transience. The timing and underlying causes of transient fluid flow, and the magnitude of associated permeability variations, remain incompletely understood.
4. Pore pressure is key to a wide range of important deformation and fluid transport processes, including the strength of faults and their mode of slip. Pore pressure magnitude is quantifiable in many cases from seismic and borehole data and is generally found to be high in wedge faults and underthrusting sediments.
5. Excess pore pressure in subduction forearcs can be viewed as a dynamic balance between (*a*) geologic forcing that acts to drive pore pressure generation and (*b*) hydraulic conductivity and drainage path length, which govern the rate of fluid escape. The magnitude of excess pressure scales approximately with the dimensionless ratio of these quantities, providing a quantitative yet simple framework for assessing overpressure development.
6. Recent work has drawn intriguing correlations between seismic reflection attributes and hydrologic and mineral dehydration processes. Where these have been studied in detail, high reflectivity appears to effectively—although qualitatively—map zones of peak dehydration and/or elevated pore pressure.
7. Pore fluid accumulations and particularly elevated fluid pressure have been linked to novel seismological and geodetic observations of fault slip, including SSE, tremors, LFE, and VLFE; low seismic velocity anomalies and a high Vp/Vs ratio provide corroborating evidence for this hypothesized linkage. However, causation, quantification, and detailed mechanisms remain to be established.
8. The updip transition into the locked and seismogenic zone may be marked by the onset of drainage of initial high overpressure, and the downdip transition may in turn mark a region where metamorphic dehydration creates a renewed pulse of fluid pressure associated with tremor and slow slip. If this speculation is correct, then the locked seismogenic zone, although weak in an absolute sense, could be relatively strong compared with the bounding transition zones.

DISCLOSURE STATEMENT

The authors are not aware of any affiliations, memberships, funding, or financial holdings that might be perceived as affecting the objectivity of this review.

ACKNOWLEDGMENTS

Much of the work described in this review grew out of research funded by the U.S. National Science Foundation (including grants 0241482, 0752114, and 0451602 to D.M.S. and grants 0241375, 0451508, 0800665, and 0800653 to H.J.T.) and by the American Chemical Society Petroleum Research Fund. We thank all our collaborators and fellow shipboard scientists over the past several years for insightful discussions that have contributed to the ideas presented here. We especially owe thanks to Casey Moore, Greg Moore, Liz Screaton, Chris Marone, Barbara Bekins, Mike Underwood, Peter Flemings, and Achim Kopf for thoughtful discussions that have been instrumental in formulating the framework and conceptual models described in this review; to Matthew Knuth for assistance with figures; to Rachel Lauer for providing images and modeling results used in **Figure 6**; to Tom Shipley and Nathan Bangs for providing original graphics to be used in **Figure 4**; and to Evan Solomon for data used to generate **Figure 5**. Owing to length restrictions, the literature cited could not encompass all the important research on the topic of fluids in subduction zones; we apologize to authors whose work we were unable to include.

LITERATURE CITED

Audet P, Bostock MG, Christensen NI, Peacock SM. 2009. Seismic evidence for overpressured subducted oceanic crust and megathrust fault sealing. *Nature* 457:76–78

Bailey EH, Irwin WP, Jones DL. 1964. Franciscan and related rocks. *Calif. Dep. Mines Geol. Bull.* 183:177

Bangs NLB, Moore GF, Gulick SPS, Pangborn EM, Tobin HJ, et al. 2009. Broad, weak regions of the Nankai megathrust and implications for shallow coseismic slip. *Earth Planet. Sci. Lett.* 284:44–49

Bangs NLB, Shipley TH, Gulick SPS, Moore GF, Kuromoto S, Nakamura Y. 2004. Evolution of the Nankai Trough décollement from the trench into the seismogenic zone: inferences from three-dimensional seismic reflection imaging. *Geology* 32:273–76

Bangs NLB, Shipley TH, Moore JC, Moore GF. 1999. Fluid accumulation and channeling along the northern Barbados Ridge décollement thrust. *J. Geophys. Res.* 104:20399–414

Bangs NLB, Westbrook GK, Ladd JW, Buhl P. 1990. Seismic velocities from the Barbados Ridge Complex: indicators of high pore fluid pressures in an accretionary complex. *J. Geophys. Res.* 95:8767–82

Barker DHN, Sutherland R, Henrys S, Bannister S. 2009. Geometry of the Hikurangi subduction thrust and upper plate, North Island, New Zealand. *Geochem. Geophys. Geosyst.* 10:Q02007

Becker K, Fisher AT, Davis EE. 1997. The CORK experiment in hole 949C: long-term observations of pressure and temperature in the Barbados accretionary prism. *Proc. Ocean Drill. Program Sci. Results*, ed. TH Shipley, Y Ogawa, P Blum, JM Bahr, 156:247–52. College Station, TX: Ocean Drill. Program

Bekins BA, Dreiss SJ. 1992. A simplified analysis of parameters controlling dewatering in accretionary prisms. *Earth Planet. Sci. Lett.* 109:275–87

Bekins BA, Matmon D, Screaton EJ, Brown KM. 2011. Reanalysis of in situ permeability measurements in the Barbados décollement. *Geofluids* 11:57–70

Bekins BA, McCaffrey AM, Dreiss SJ. 1994. The influence of kinetics on the smectite to illite transition in the Barbados accretionary prism. *J. Geophys. Res.* 99:18147–58

Bekins BA, McCaffrey AM, Dreiss SJ. 1995. Episodic and constant flow models for the origin of low-chloride waters in a modern accretionary complex. *Water Resour. Res.* 31(12):3205–15

Bekins BA, Screaton EJ. 2007. Pore pressure and fluid flow in the northern Barbados accretionary complex. In *The Seismogenic Zone of Subduction Thrust Faults*, ed. TH Dixon, JC Moore, pp. 148–70. New York: Columbia Univ. Press

Bell R, Sutherland R, Barker DHN, Henrys S, Bannister S, et al. 2010. Seismic reflection character of the Hikurangi subduction interface, New Zealand, in the region of repeated Gisborne slow slip events. *Geophys. J. Int.* 180(1):34–48

Bethke CM. 1986. Inverse hydrogeologic analysis of the distribution and origin of Gulf Coast–type geopressured zones. *J. Geophys. Res.* 91:6535–45

Bourlange S, Henry P. 2007. Numerical model of fluid pressure solitary wave propagation along the décollement of an accretionary wedge: application to the Nankai wedge. *Geofluids* 7(3):323–34

Bray CJ. Karig DE. 1985. Porosity of sediments in accretionary prisms and some implications for dewatering processes. *J. Geophys. Res.* 90:768–78

Brown KM, Bekins B, Clennell B, Dewhurst D, Westbrook G. 1994. Heterogeneous hydrofracture development and accretionary fault dynamics. *Geology* 22(3):259–62

Brown KM, Tryon M, DeShon H, Dorman L, Schwartz S. 2005. Correlated transient fluid pulsing and seismic tremor in the Costa Rica subduction zone. *Earth Planet. Sci. Lett.* 238(1):189–203

Bruce CH. 1984. Smectite dehydration—its relations to structural development and hydrocarbon accumulation in northern Gulf of Mexico basin. *AAPG Bull.* 68:673–83

Byrne T, Fisher D. 1990. Evidence for a weak and overpressured décollement beneath sediment-dominated accretionary prisms. *J. Geophys. Res.* 95:9081–97

Calahorrano AB, Sallares V, Collot J-Y, Sage F, Ranero CR. 2008. Nonlinear variations of the physical properties along the southern Ecuador subduction channel: results from depth-migrated seismic data. *Earth Planet. Sci. Lett.* 267(3–4):453–67

Carson B, Screaton EJ. 1998. Fluid flow in accretionary prisms: evidence for focused, time-variable discharge. *Rev. Geophys.* 36:329–51

Cochrane GR, Moore JC, MacKay ME, Moore GF. 1994. Velocity and inferred porosity model of the Oregon accretionary prism from multichannel seismic reflection data: implications on sediment dewatering and overpressure. *J. Geophys. Res.* 99:7033–43

Connolly JAD. 2010. The mechanics of metamorphic fluid expulsion. *Elements* 6:165–72

Cutillo PA, Screaton EJ, Ge S. 2003. Three-dimensional numerical simulation of fluid flow and heat transport within the Barbados Ridge accretionary complex. *J. Geophys. Res.* 108:2555

Davis D, Suppe J, Dahlen FA. 1983. Mechanics of fold-and-thrust belts and accretionary wedges. *J. Geophys. Res.* 88:1153–72

Davis EE, Becker K, Wang K, Obara K, Ito Y, Kinoshita M. 2006. A discrete episode of seismic and aseismic deformation of the Nankai trough subduction zone accretionary prism and incoming Philippine Sea plate. *Earth Planet. Sci. Lett.* 242:73–84

Davis EE, Hyndman RD, Villinger H. 1990. Rates of fluid expulsion across the northern Cascadia accretionary prism: constraints from new heat flow and multichannel seismic reflection data. *J. Geophys. Res.* 95(B6):8869–89

Davis EE, Villinger HW. 2006. Transient formation fluid pressures and temperatures in the Costa Rica forearc prism and subducting oceanic basement: CORK monitoring at ODP Sites 1253 and 1255. *Earth Planet. Sci. Lett.* 245(1–2):232–44

Dean SM, McNeill LC, Henstock TJ, Bull JM, Gulick SPS, et al. 2010. Contrasting décollement and prism properties over the Sumatra 2004–2005 earthquake rupture boundary. *Science* 329(5988):207–10

Deyhle A, Kopf A, Aloisi G. 2003. Boron and boron isotopes as a tracer for diagenetic reactions and depth of mobilization, using muds and authigenic carbonates from eastern Mediterranean mud volcanoes. *Geol. Soc. Lond. Spec. Publ.* 216:493–505

Fagereng A, Ellis S. 2009. On factors controlling the depth of interseismic coupling on the Hikurangi subduction interface, New Zealand. *Earth Planet. Sci. Lett.* 278:120–30

Fisher AT, Hounslow MW. 1990. Transient fluid flow through the toe of the Barbados accretionary complex: constraints from Ocean Drilling Program Leg 110 heat flow studies and simple models. *J. Geophys. Res.* 95:8845–58

Fisher AT, Zwart G. 1996. Relation between permeability and effective stress along a plate-boundary fault, Barbados accretionary complex. *Geology* 24:307–10

Fisher D, Brantley S, Everett M, Dzvonik J. 1995. Cyclic fluid flow through a regionally extensive fracture network within the Kodiak accretionary prism. *J. Geophys. Res.* 100(B7):12881–94

Flemings PB. 2002. Overpressures above the décollement at Nankai: ODP Sites 808 and 1174. *Eos Trans. AGU* 83(47), Fall Meet. Suppl., Abstr. H22E–08
Frey M, Robinson D, eds. 1999. *Low-Grade Metamorphism*. Oxford: Blackwell Sci. 328 pp.
Fyfe WS, Price NJ, Thompson AB. 1978. *Fluids in the Earth's Crust*. Amsterdam: Elsevier. 383 pp.
Gamage K. Screaton E. 2006. Characterization of excess pore pressures at the toe of the Nankai accretionary complex, Ocean Drilling Program sites 1173, 1174, and 808: results of one-dimensional modeling. *J. Geophys. Res.* 111:B04103
Gettemy GL, Tobin HJ. 2003. Tectonic signatures in centimeter-scale velocity-porosity relationships of Costa Rica convergent margin sediments. *J. Geophys. Res.* 108:2494–505
Gettemy GL, Tobin HJ, Hole JA, Sayed AY. 2004. Multiscale compressional wave velocity structure of the San Gregorio Fault zone. *Geophys. Res. Lett.* 31:L06601
Gomberg J. 2010. Introduction to special section on phenomenology, underlying processes, and hazard of aseismic slip and nonvolcanic tremor. *J. Geophys. Res.* 115:B00A00
Gorman PJ, Kerrick DM, Connolly JAD. 2006. Modeling open system metamorphic decarbonation of subducting slabs. *Geochem. Geophys. Geosyst.* 7:Q04007
Hacker BR. 2008. H_2O subduction beyond arcs. *Geochem. Geophys. Geosyst.* 9:Q03001
Hacker BR, Abers GA, Peacock SM. 2003. Subduction factory 1. Theoretical mineralogy, densities, seismic wave speeds, and H_2O contents. *J. Geophys. Res.* 108:2029
Hanson RB. 1992. Effects of fluid production on fluid flow during regional and contact metamorphism. *J. Metamorph. Geol.* 10:87–98
Henry P. 2000. Fluid flow at the toe of the Barbados accretionary wedge constrained by thermal, chemical, and hydrogeologic observations and models. *J. Geophys. Res.* 105:25855–72
Henry P, Lallemant S, Nakamura K, Tsunogai U, Mazzotti S, Kobayashi K. 2002. Surface expression of fluid venting at the toe of the Nankai wedge and implications for flow paths. *Mar. Geol.* 187:119–43
Henry P, Wang C-Y. 1991. Modeling of fluid flow and pore pressure at the toe of Oregon and Barbados accretionary wedges. *J. Geophys. Res.* 96(B12):20109–30
Hensen C, Wallmann K. 2005. Methane formation at Costa Rica continental margin—constraints for gas hydrate inventories and cross-décollement fluid flow. *Earth Planet. Sci. Lett.* 236:41–60
Hensen C, Wallmann K, Schmidt M, Ranero C, Suess E. 2004. Fluid expulsion related to mud extrusion off Costa Rica—a window to the subducting slab. *Geology* 32(2):201–4
Hubbert MK, Rubey WW. 1959. Role of fluid pressure in mechanics of overthrust faulting. *Geol. Soc. Am. Bull.* 70:115–66
Ide S, Beroza GC, Shelly DR, Uchide T. 2007. A scaling law for slow earthquakes. *Nature* 447:76–79
Ikari MJ, Saffer DM, Marone C. 2009. Frictional and hydrologic properties of clay rich fault gouge. *J. Geophys. Res.* 114:B05409
Ito Y, Obara K. 2006. Very low frequency earthquakes within accretionary prisms are very low stress-drop earthquakes. *Geophys. Res. Lett.* 33:L09302
Johnson P, McEvilly T. 1995. Parkfield seismicity: fluid-driven? *J. Geophys. Res.* 100(B7):12937–50
Kao H, Shan S-Ju, Rogers G, Dragert H, Cassidy JF, Ramachandran K. 2005. Depth distribution of seismic tremors along the northern Cascadia margin. *Nature* 436:841–44
Karig DE. 1990. Experimental and observational constraints on the mechanical behaviour in the toes of accretionary prisms. *Geol. Soc. Lond. Spec. Publ.* 54:383–93
Kastner M, Elderfield H, Martin JB. 1991. Fluids in convergent margins: What do we know about their composition, origin, role in diagenesis and importance for oceanic chemical fluxes? *Philos. Trans. R. Soc. Lond. Ser. A* 335:243–59
Kato A, Iidaka T, Ikuta R, Yoshida Y, Katsumata K, et al. 2010. Variations of fluid pressure within the subducting oceanic crust and slow earthquakes. *Geophys. Res. Lett.* 37:L14310
Kato A, Sakaguchi A, Yoshida S, Yamaguchi H, Kaneda Y. 2004. Permeability structure around an ancient exhumed subduction-zone fault. *Geophys. Res. Lett.* 31:L06602
Kerrick DM, Connolly JAD. 2001a. Metamorphic devolatilization of subducted marine sediments and the transport of volatiles into the Earth's mantle. *Nature* 411:293–96
Kerrick DM, Connolly JAD. 2001b. Metamorphic devolatilization of subducted oceanic metabasalts: implications for seismicity, arc magmatism, and volatile recycling. *Earth Planet. Sci. Lett.* 189:19–29

Kimura G, Silver E, Blum P, et al. 1997. *Proc. Ocean Drill. Program Initial Rep.*, Vol. 170. College Station, TX: Ocean Drill. Program. 554 pp.
Kodaira S, Iidaka T, Kato A, Park JO, Iwasaki T, Kaneda Y. 2004. High pore fluid pressure may cause silent slip in the Nankai Trough. *Science* 304:1295–98
Kondo H, Kimura G, Masago H, Ohmori-Ikehara K, Kitamura Y, et al. 2005. Deformation and fluid flow of a major out-of-sequence thrust located at seismogenic depth in an accretionary complex: Nobeoka thrust in the Shimanto Belt, Kyushu, Japan. *Tectonics* 24:TC6008
Kopf A, Mora G, Deyhle A, Frape S, Hesse R. 2003. Fluid geochemistry in the Japan Trench forearc (ODP Leg 186): a synthesis. *Proc. Ocean Drill. Program Sci. Results*, ed. K Suyehiro, IS Sacks, GD Acton, M Oda, 186:1–23. College Station, TX: Ocean Drill. Program
Kopf AJ. 2002. Significance of mud volcanism. *Rev. Geophys.* 40(2):1005–57
Kwon O, Kronenberg AK, Gangi AF, Johnson B, Herbert BE. 2004. Permeability of illite-bearing shale: 1. Anisotropy and effects of clay content and loading. *J. Geophys. Res.* 109:B10205
Labaume P, Kastner M, Trave A, Henry P. 1997. Carbonate veins from the décollement zone at the toe of the northern Barbados accretionary prism: microstructure, mineralogy, geochemistry, and relations with prism structures and fluid regime. *Proc. Ocean Drill. Program Sci. Results*, ed. TH Shipley, Y Ogawa, P Blum, JM Bahr, 156:79–96. College Station, TX: Ocean Drill. Program
Lallemand S, Schnürle P, Malavieille J. 1994. Coulomb theory applied to accretionary and nonaccretionary wedges: possible causes for tectonic erosion and/or frontal accretion. *J. Geophys. Res.* 99(B6):12033–55
Lauer RM, Saffer DM. 2010. The impact of splay faults on the geochemistry and fluid budget of a subduction zone. *Geophys. Res. Abstr.* 12:EGU2010–13243 (Abstr.)
Linke P, Suess E, Torres M, Martens V, Rugh WD, et al. 1994. In situ measurement of fluid flow from cold seeps at active continental margins. *Deep Sea Res. Part I* 41(4):721–39
Liu Y, Rice JR. 2007. Spontaneous and triggered aseismic deformation transients in a subduction fault model. *J. Geophys. Res.* 112:B09404
Magee ME, Zoback MD. 1993. Evidence for a weak interplate thrust fault along the northern Japan subduction zone and implications for the mechanics of thrust faulting and fluid expulsion. *Geology* 21(9):809–12
Matmon D, Bekins BA. 2006. Hydromechanics of a high taper angle, low-permeability prism: a case study from Peru. *J. Geophys. Res.* 111:B07101
Moore GF, Shipley TH, Stoffa PL, Karig DE, Taira A, et al. 1990. Structure of the Nankai Trough accretionary zone from multichannel seismic reflection data. *J. Geophys. Res.* 95:8753–65
Moore JC. 1989. Tectonics and hydrogeology of accretionary prisms: role of the décollement zone. *J. Struct. Geol.* 11:95–106
Moore JC, Tobin H. 1997. Estimated fluid pressures of the Barbados accretionary prism and adjacent sediments. *Proc. Ocean Drill. Program Sci. Results*, ed. TH Shipley, Y Ogawa, P Blum, JM Bahr, 156:229–38. College Station, TX: Ocean Drill. Program
Moore JC, Vrolijk P. 1992. Fluids in accretionary prisms. *Rev. Geophys.* 30:113–35
Morgan JK, Karig DE. 1993. Ductile strains in clay-rich sediment from Hole 808C: preliminary results using X-ray pole figure goniometry. *Proc. Ocean Drill. Program Sci. Results*, ed. IA Hill, A Taira, JV Firth, et al., 131:141–55. College Station, TX: Ocean Drill. Program
Morris JD, Villinger HW, Klaus A, et al. 2003. *Proc. Ocean Drill. Program Initial Rep.*, Vol. 205. College Station, TX: Ocean Drill. Program [CD-ROM]
Neuzil CE. 1995. Abnormal pressures as hydrodynamic phenomena. *Am. J. Sci.* 295:742–86
Obana K, Kodaira S. 2009. Low-frequency tremors associated with reverse faults in a shallow accretionary prism. *Earth Planet. Sci. Lett.* 287(1–2):168–74
Oleskevich DA, Hyndman RD, Wang K. 1999. The updip and downdip limits to great subduction earthquakes: thermal and structural models of Cascadia, south Alaska, SW Japan, and Chile. *J. Geophys. Res.* 104:14965–91
Orange DL, Breen NA. 1992. The effects of fluid escape on accretionary wedges 2. Seepage force, slope failure, headless submarine canyons, and vents. *J. Geophys. Res.* 97(B6):9277–95
Park J, Fujie G, Wijerathne L, Hori T, Kodaira S, et al. 2010. A low-velocity zone with weak reflectivity along the Nankai subduction zone. *Geology* 38:283–86

Park J, Tsuru T, Takahashi N, Hori T, Kodaira S, et al. 2002. A deep strong reflector in the Nankai accretionary wedge from multichannel seismic data: implications for underplating and interseismic shear stress release. *J. Geophys. Res.* 107:2061–77

Peacock SM. 2009. Thermal and metamorphic environment of subduction zone episodic tremor and slip. *J. Geophys. Res.* 114:B00A07

Peacock SM, Hyndman RD. 1999. Hydrous minerals in the mantle wedge and the maximum depth of subduction thrust earthquakes. *Geophys. Res. Lett.* 26:2517–20

Pytte AM, Reynolds RC. 1988. The thermal transformation of smectite to illite. In *Thermal Histories of Sedimentary Basins*, ed. ND Naeser, TH McCulloh, pp. 133–40. New York: Springer-Verlag

Ranero CR, Grevemeyer I, Sahling H, Barckhausen U, Hensen C, et al. 2008. Hydrogeological system of erosional convergent margins and its influence on tectonics and interplate seismogenesis. *Geochem. Geophys. Geosyst.* 9:Q03S04

Ransom B, Spivack AJ, Kastner M. 1995. Stable Cl isotopes in subduction-zone pore waters: implications for fluid-rock reactions and the cycling of chlorine. *Geology* 23(8):715–18

Rice JR. 1992. Fault stress states, pore pressure distributions, and the weakness of the San Andreas fault. In *Fault Mechanics and Transport Properties of Rocks*, ed. B Evans, TF Wong, pp. 475–503. San Diego, CA: Academic

Rowe CD, Meneghini F, Moore JC. 2009. Fluid-rich damage zone of an ancient out-of-sequence thrust, Kodiak Islands, Alaska. *Tectonics* 28:TC1006

Saffer DM. 2003. Pore pressure development and progressive dewatering in underthrust sediments at the Costa Rica subduction margin: comparison with northern Barbados and Nankai. *J. Geophys. Res.* 108(B5):2261

Saffer DM. 2010. Hydrostratigraphy as a control on subduction zone mechanics through its effects on drainage: an example from the Nankai margin, SW Japan. *Geofluids* 10(1–2):114–31

Saffer DM, Bekins BA. 1998. Episodic fluid flow in the Nankai accretionary complex: timescale, geochemistry, and fluid budget. *J. Geophys. Res.* 103:30351–70

Saffer DM, Bekins BA. 1999. Fluid budgets at convergent plate margins: implications for the extent and duration of fault-zone dilation. *Geology* 29:1095–98

Saffer DM, Bekins BA. 2002. Hydrologic controls on the morphology and mechanics of accretionary wedges. *Geology* 30:271–74

Saffer DM, Bekins BA. 2006. An evaluation of factors influencing pore pressure in accretionary complexes: implications for taper angle and wedge mechanics. *J. Geophys. Res.* 111:B04101

Saffer DM, McKiernan AW. 2005. Permeability of underthrust sediments at the Costa Rican margin: scale dependence and implications for dewatering. *Geophys. Res. Lett.* 32:L02302

Saffer DM, Underwood MB, McKiernan AW. 2008. Evaluation of factors controlling smectite transformation and fluid production in subduction zones: application to the Nankai Trough. *Isl. Arc* 17:208–30

Sahling H, Masson DG, Ranero CR, Hühnerbach V, Weinrebe W, et al. 2008. Fluid seepage at the continental margin offshore Costa Rica and southern Nicaragua. *Geochem. Geophys. Geosyst.* 9:Q05S05

Saito S, Goldberg D. 2001. Compaction and dewatering processes of the oceanic sediments in the Costa Rica and Barbados subduction zones: estimates from in situ physical properties measurements. *Earth Planet. Sci. Lett.* 191:283–93

Scholz CH. 1998. Earthquakes and friction laws. *Nature* 391:37–42

Schwartz SY, DeShon HR. 2007. Distinct updip limits to geodetic locking and microseismicity at the Northern Costa Rican seismogenic zone. In *The Seismogenic Zone of Subduction Thrust Faults*, ed. T Dixon, JC Moore, pp. 576–99. New York: Columbia Univ. Press

Screaton E, Carson B, Davis E, Becker K. 2000. Permeability of a décollement zone: results from a two-well experiment in the Barbados accretionary complex. *J. Geophys. Res.* 105(B9):21403–10

Screaton E, Carson B, Lennon G. 1995. Hydrogeologic properties of a thrust fault within the Oregon Accretionary Prism. *J. Geophys. Res.* 100(B10):20025–35

Screaton E, Ge S. 1997. An assessment of along-strike fluid and heat transport within the Barbados Ridge accretionary complex: results of preliminary modeling. *Geophys. Res. Lett.* 24:3085–88

Screaton EJ, Saffer DM, Henry P, Hunze S. 2002. Porosity loss within the underthrust sediments of the Nankai accretionary complex: implications for overpressures. *Geology* 30:19–22

Screaton EJ, Wuthritch DR, Dreiss SJ. 1990. Permeabilities, fluid pressures, and flow rates in the Barbados Ridge complex. *J. Geophys. Res.* 95:8997–9007
Shelly DR, Beroza GC, Ide S, Nakamura S. 2006. Low frequency earthquakes in Shikoku, Japan, and their relationship to episodic tremor and slip. *Nature* 442:188–91
Shipley TH, Moore GF, Bangs NL, Moore JC, Stoffa PL. 1994. Seismically inferred dilatancy distribution, northern Barbados ridge décollement: implications for fluid migration and fault strength. *Geology* 22:411–14
Sibson RH, Rowland JV. 2003. Stress, fluid pressure and structural permeability in seismogenic crust, North Island, New Zealand. *Geophys. J. Int.* 154:584–94
Skarbek RM, Saffer DM. 2009. Pore pressure development beneath the décollement at the Nankai subduction zone: implications for plate boundary fault strength and sediment dewatering. *J. Geophys. Res.* 114:B07401
Solomon EA, Kastner M, Wheat G, Jannasch HW, Robertson G, et al. 2009. Long-term hydrogeochemical records in the oceanic basement and forearc prism at the Costa Rica subduction zone. *Earth Planet. Sci. Lett.* 282:240–51
Song TA, Helmberger DV, Brudzinski MR, Clayton RW, Davis P, et al. 2009. Subducting slab ultra-slow velocity layer coincident with silent earthquakes in southern Mexico. *Science* 324:502–6
Spinelli GA, Saffer DM. 2004. Along-strike variations in underthrust sediment dewatering on the Nicoya margin, Costa Rica, related to the updip limit of seismicity. *Geophys. Res. Lett.* 31:L04613
Spinelli GA, Saffer DM. 2007. Trench-parallel fluid flow in subduction zones resulting from temperature differences. *Geochem. Geophys. Geosyst.* 8:Q09009
Spinelli GA, Saffer DM, Underwood MB. 2006. Hydrogeologic responses to three-dimensional temperature variability, Costa Rica subduction margin. *J. Geophys. Res.* 111:B04403
Spinelli GA, Wang K. 2008. Effects of fluid circulation in subducting crust on Nankai margin seismogenic zone temperatures. *Geology* 36(11):887–90
Suppe J. 1981. Mechanics of mountain building and metamorphism in Taiwan. *Mem. Geol. Soc. China* 4:67–89
Teichert BMA, Torres ME, Bohrmann G, Eisenhauer A. 2005. Fluid sources, fluid pathways and diagenetic reactions across an accretionary prism revealed by Sr and B geochemistry. *Earth Planet. Sci. Lett.* 239:106–21
Tobin HJ, Moore JC, Moore GF. 1994. Fluid pressure in the frontal thrust of the Oregon accretionary prism: experimental constraints. *Geology* 22(11):979–82
Tobin HJ, Saffer DM. 2009. Elevated fluid pressure and extreme mechanical weakness of a plate boundary thrust, Nankai Trough subduction zone. *Geology* 37:679–82
Tobin HJ, Vannucchi P, Meschede M. 2001. Structure, inferred mechanics, and implications for fluid transport in the décollement zone, Costa Rica convergent margin. *Geology* 29:907–10
Torres ME, Teichert BMA, Tréhu AM, Borowski W, Tomaru H. 2004. Relationship of pore water freshening to accretionary processes in the Cascadia margin: fluid sources and gas hydrate abundance. *Geophys. Res. Lett.* 31:L22305
Tryon MD, Wheat CG, Hilton DR. 2010. Fluid sources and pathways of the Costa Rica erosional convergent margin. *Geochem. Geophys. Geosyst.* 11:Q04S22
Tsuji T, Tokuyama H, Costa Pisani P, Moore G. 2008. Effective stress and pore pressure in the Nankai accretionary prism off the Muroto Peninsula, southwestern Japan. *J. Geophys. Res.* 113:B11401
Tsuru T, Park JO, Kido Y, Ito A, Kaneda Y, et al. 2005. Did expanded porous patches guide rupture propagation in 2003 Tokachi-oki earthquake? *Geophys. Res. Lett.* 32:L20310
Underwood MB. 2007. Sediment inputs to subduction zones: why lithostratigraphy and clay mineralogy matter. In *The Seismogenic Zone of Subduction Thrust Faults*, ed. TH Dixon, JC Moore, pp. 42–85. New York: Columbia Univ. Press
Underwood MB, Laughland MM, Kang SM. 1993. A comparison among organic and inorganic indicators of diagenesis and low-temperature metamorphism, Tertiary Shimanto Belt, Shikoku, Japan. *Geol. Soc. Am. Spec. Pap.* 273:45–61
von Huene R, Scholl DW. 1991. Observations at convergent margins concerning sediment subduction, subduction erosion, and the growth of continental crust. *Rev. Geophys.* 29:279–316
Wada I, Wang K, He J, Hyndman RD. 2008. Weakening of the subduction interface and its effects on surface heat flow, slab dehydration, and mantle wedge serpentinization. *J. Geophys. Res.* 113:B04402

Wang K. 1994. Kinematic models of dewatering accretionary prisms. *J. Geophys. Res.* 99:4429–38
Westbrook GK. 1991. Geophysical evidence for the role of fluids in accretionary wedge tectonics. *Philos. Trans. R. Soc. Lond. Ser. A* 335:227–42
Wong T-F, Ko S-C, Olgaard DL. 1997. Generation and maintenance of pore pressure excess in a dehydrating system 2. Theoretical analysis. *J. Geophys. Res.* 102:841–52
Zwart G, Brückmann W, Moran K, MacKillop AK, Maltman AJ, et al. 1997. Evaluation of hydrogeologic properties of the Barbados accretionary prism: a synthesis of Leg 156 results. *Proc. Ocean Drill. Program Sci. Results*, ed. TH Shipley, Y Ogawa, P Blum, JM Bahr, 156:303–10. College Station, TX: Ocean Drill. Program
Zwart G, Moore JC, Cochrane GR. 1996. Variations in temperature gradients identify active faults in the Oregon accretionary prism. *Earth Planet. Sci. Lett.* 139:485–95

Annual Review
of Earth and
Planetary Sciences
Volume 39, 2011

Contents

Indexes

Errata

An online log of corrections to *Annual Review of Earth and Planetary Sciences* articles may be found at http://earth.annualreviews.org